

# Journal Pre-proof

Robust adaptive nonsingular fast terminal sliding-mode tracking control for an uncertain quadrotor UAV subjected to disturbances

Moussa Labbadi, Mohamed Cherkaoui



PII: S0019-0578(19)30466-5

DOI: <https://doi.org/10.1016/j.isatra.2019.10.012>

Reference: ISATRA 3385

To appear in: *ISA Transactions*

Received date: 26 February 2019

Revised date: 28 October 2019

Accepted date: 28 October 2019

Please cite this article as: M. Labbadi and M. Cherkaoui, Robust adaptive nonsingular fast terminal sliding-mode tracking control for an uncertain quadrotor UAV subjected to disturbances. *ISA Transactions* (2019), doi: <https://doi.org/10.1016/j.isatra.2019.10.012>.

This is a PDF file of an article that has undergone enhancements after acceptance, such as the addition of a cover page and metadata, and formatting for readability, but it is not yet the definitive version of record. This version will undergo additional copyediting, typesetting and review before it is published in its final form, but we are providing this version to give early visibility of the article. Please note that, during the production process, errors may be discovered which could affect the content, and all legal disclaimers that apply to the journal pertain.

© 2019 Published by Elsevier Ltd on behalf of ISA.



**Moussa Labbadi** received the M.S. degrees in Mechatronic from University Abdelmalek Essaadi of Tetouan, Morocco, in 2017. Currently, he is a Ph.D. student at the Engineering for Smart and Sustainable Systems Research Center (E3S) of Mohammadia School of Engineers, Mohammed V University, Rabat, Morocco. His research interests include Robotics, Aerial Robotics (Quadrotor UAV Drones), Mechatronics (Motion control smart machines), Estimation, Nonlinear control, sliding mode control and aerospace vehicles.



**Mohamed Cherkaoui** was born in Marrakech, Morocco, in 1954. He received the state engineer degree in electrical engineering from the Mohammadia School of Engineers, Mohammed V University, Rabat, Morocco, in 1979 and the M.Sc.A. and Ph.D. degrees from the National Polytechnique Institute of Lorraine, Nancy, France, in 1983 and 1990, respectively, all in Electrical Engineering. During 1990-1994, he was an Assistant Professor in Physical department, Kadi Ayyad university, Marrakech, Morocco. In 1995, he joined the Department of Electrical Engineering, Mohammadia School of Engineers, Mohammed V University in Rabat, Morocco, where is currently a Professor and University Research Professor. He is director of Engineering For Smart and Sustainable Systems Research Center (E3S). He has published more than 100 scientific journal articles and conference papers. His current research interests include renewable energy, motor drives, power electronics, electrical machine, unmanned aerial vehicle systems and nonlinear control.

The contributions of this research are given as follows:

- High precision tracking performance of a quadrotor with known or unknown perturbations and fast convergence are achieved by the proposed approach.
  - Good robustness is provided against various external disturbances, modelling uncertainties and noise measurements.
  - Without previous knowledge of uncertainty and disturbances, the adaptive self-tuning laws are designed to estimate the unknown upper bounds of them.
  - The singularity problem in the adaptive TSM control and the chattering phenomenon in SM control are avoided by the RANFTSMC strategy.

# Robust adaptive nonsingular fast terminal sliding-mode tracking control for an uncertain quadrotor UAV subjected to disturbances

Moussa Labbadi<sup>a</sup>, Mohamed Cherkaoui<sup>a</sup>

<sup>a</sup> Mohammed V University in Rabat, Engineering 3S Research Center, Mohammadia School of Engineers, Rabat, Morocco

## Abstract

This paper investigates the design of a robust controller for the trajectory tracking problem of an under-actuated quadrotor UAV subject to the modeling uncertainties and unknown external disturbances. A new robust nonlinear adaptive controller is proposed for orientation and translation tracking by using the Adaptive Nonsingular Fast Terminal Sliding-Mode Control (ANFTSMC) algorithms. The ANFTSM control law: **(i)** ensures fast convergence, i.e. the quadrotor outputs achieve to the original values in a short finite-time; **(ii)** avoids singularities; **(iii)** solves the chattering effect; **(iv)** offers robustness against the unknown external disturbances and uncertainties. Furthermore, the system unknown uncertainty and external disturbances upper bound are coped by the proposed control approach. Online estimation of these upper bounds is only introduced by velocity and position measurements. In addition, the control law applies the Lyapunov theory, guarantees the closed-loop stability of the quadrotor system. Finally, various simulations under different scenarios in terms of external disturbances and parametric uncertainties are carried out to evaluate/emphasize the effectiveness of the ANFTSMC strategy proposed in this work. Moreover, a comparative study is accomplished at the end of the present paper and shows clearly the outperformance of the proposed control scheme.

\*Corresponding author  
Email address: [moussalabbadi@research.emi.ac.ma](mailto:moussalabbadi@research.emi.ac.ma) (Moussa Labbadi<sup>a</sup>)

*Keywords:* Nonsingular fast terminal sliding-mode, Quadrotor UAVs, Attitude and position control, Uncertainties and disturbances, Adaptive laws

## 1. Introduction

### 1.1. Context and Motivations

The unmanned aerial vehicle research becomes an interesting topic during the last years. These drones offer great flexibility of use for both the military and civil missions. Advancement in electric power storage, embedded hardware design, material structures, electronics, computing sciences, and real-time processing have led to the introduction of innovative drones. The quadrotor can be considered as one of the most nascent drones and many applications/implementations have been fulfilled by this type of vehicle, their applications cover a wide range of fields such as mailing and delivery, environmental protection, search/rescue, monitoring, reconnaissance inside buildings, maintenance, agriculture, videography/photography, miming, nuclear, biological, and chemical operations [1]. The quadrotor can be used either in indoor- or outdoor-flight under different environments (underwater, over water surface, ground, air, and space) [1]. In contrast to some conventional helicopters, quadrotors seem to be more attractive. They have a lightweight structure and a simple mechanical design, which allows stable hover flight [2]. In addition, they can move along a target in close quarters, vertically take-off and move in cluttered small areas [2]. The quadrotor can assist humans in everyday life and also in a large spectrum of tasks, especially those expose some difficulties and hazards [2]. In spite of all these advantages, quadrotors have some major issues mainly/partly related to their propeller rotation and blades flapping [3]. In addition, the position and attitude are strongly coupled, which increases the complexity of the quadrotor control system; it is typically under-actuated with disturbances due to the aerodynamic effects, and sensitive to a wind gust, which leads to instability [4]. By controlling a quadrotor, three challenges should be addressed [4, 5]: (1) the dynamic of the quadrotor is a multi-output multi-input (MIMO) system; (2)

the position and attitude dynamics involve unmodeled uncertainties, external perturbations, and parametric uncertainties; (3) multiple-input time delays and time-varying states. In order to compensate an external perturbations and to improve the quadrotor trajectory tracking performances, many robust nonlinear control approaches have been designed the aforementioned problems, like as a robust backstepping output feedback [6], fractional-order PID control [7], damping assignment-passivity based control and an interconnection strategy [8], sliding mode backstepping controller [9, 10], disturbance observer [11], continuous sliding-modes control strategies [12], adaptive sliding mode tracking control with disturbances algorithms [13], nonlinear high-gain observer and 2-order sliding mode control algorithms [14], adaptive and robust control with input saturation [15], novel robust PID-type controller [16], fractional sliding mode controller in finite-time technique [17], and global fast terminal SMC technique [18].

### *1.2. Related Work*

The authors in Ref. [19] propose a survey study, of the nonlinear controllers (Model predictive, Backstepping, Feedback linearization, and sliding mode) and intelligent methods (Fuzzy logic and neural network), is presented. The authors have elaborated a comparative study and highlighted both the advantages and disadvantages of each technique used for the flight controller to drive a quadrotor. With regard to the results obtained from the comparative study, adaptive terminal sliding mode control method was considered as the best suitable approach for quadrotor system. In Ref. [20], a generalized dynamic inversion design is proposed for the quadrotor position trajectory. The attitude loop uses a robust control of a nonlinear terminal SMC method. In Ref. [21], the quadrotor model was obtained by using Lagrange-Euler method. A predictive control strategy with integral action is developed to track position trajectory and  $H_\infty$  control is designed to stabilize the quadrotor orientation. The work developed in Ref. [22] dealt with path tracking problem under aerodynamic moments and forces by using the integral backstepping and nonlinear  $H_\infty$ . In the

case of the quadrotor's payload variation, a hierarchical nonlinear control based on the thrust allocation algorithm and the Lyapunov technique is developed in Ref. [3]. In Ref. [23], the authors propose a robust control method to improve the quadrotor position tracking performance, which is based on a second-order SMC approach. In Ref. [24], the path tracking problem the quadrotor UAV was investigated by designing a combination between hybrid model predictive and fuzzy logic controllers. The external disturbances and unknown states of the quadrotor are estimated using an observer in Ref. [25]. In order to estimate the total disturbances and to control of the quadrotor, an active disturbance rejection control based on virtual variables is designed in Ref. [26]. In Ref. [27], robust nonlinear controllers are proposed to control the quadrotor subjected to the uncertainties, noises, and disturbances. The attitude loop control uses the terminal SMC with integral backstepping approach and the outer loop uses a robust PID controller. In Ref. [28], a geometric control theory addressed the problem of designing a controller for the quadrotor system with actuation constraints. In Ref. [29], three control methods are designed for the quadrotor MAV based on linear and nonlinear optimal control theory. Reference [30] presents an observer for the quadrotor pitch/roll angles subjected to complex disturbances, which is based on sliding mode algorithms. Reference [31] proposes a model via Lagrange-Euler formalism and controlling based on damping assignment-passivity of the quadrotor system. In Ref. [32], a visual mechanism control based on artificial neural networks to control a quadrotor attitude and position is designed. A hybrid finite-time control technique is presented in Ref. [33], which is based on an adaptive integral SMC, backstepping, and nonsingular terminal SMC approaches to resolve the quadrotor path tracking problems with unknown dynamics and perturbations. In Ref. [34], a cascade control is proposed using a PID controller and Lyapunov analysis to stabilize the quadcopter. As for the under-actuated architecture of the quadrotor, SMC and terminal SMC methods are proposed to ensure the vehicle stabilization control in Ref. [35]. Reference [36] proposes a robust hierarchical control technique based on neural networks and SMC for dealing with the quadrotor control

under parametric uncertainty and disturbances. In Ref. [5], an adaptive SMC finite-time control method is suggested for controlling the quadrotor system. A procedure estimation of the parametric uncertainty is proposed. In Ref. [37], an internal model control approach has been proposed to stabilize the quadrotor. The wind gust perturbations, affecting the vehicle, have been coped in the presence of the sensor fault and uncertainties.

### 1.3. Contribution

In the present work, a robust flight controller for a quadrotor position and attitude is developed. The objective of this control strategy is to stabilize the attitude of the vehicle and to follow the flight path of the quadrotor in a short finite time, where the quadrotor system considered has uncertain parameters and is affected by a gust of wind in the presence of noise in sensors. The overall closed-loop stability of the vehicle and the global convergence of the position and attitude tracking errors are obtained according the Lyapunov analysis and theory. A new robust adaptive SMC mixed with a nonsingular fast terminal sliding surface is employed for dealing with the quadrotor position trajectory tracking problem and stabilize the attitude loop of this vehicle against the disturbances. An adaptive gain-tuning method is developed to estimate the unknown upper bounds of the disturbances, which affect the attitude and position dynamics. The numerical simulations of the proposed ANFTSMC approach of the vehicle attitude and position confirm higher stabilization accuracy, lower values of performance indices, and good tracking of many proposed complex flight trajectories. The suggested technique is compared with other robust control methods in different scenarios. The chattering problem is solved without losing the trajectory tracking performance and robustness against the disturbances.

The main contributions of this paper are as follows:

- High precision tracking performances of a quadrotor with known or unknown perturbations and fast convergence are achieved by the proposed approach.

- Good robustness is provided against various external disturbances, modeling uncertainties and noise measurements.
- Without previous knowledge of uncertainty and disturbances, the adaptive self-tuning laws are proposed to estimate the unknown upper bounds of them.
- The singularity problem in the adaptive TSM control and the chattering phenomena in SM control are avoided by the RANFTSMC strategy.

#### *1.4. Structure of the Manuscript*

The remainder of this paper is organized as follows. A system model formulation is given in [Section 2](#). The RANFTSMC proposed in this paper, for controlling the quadrotor subjected to the disturbances and bounded uncertainties of their parameters, is given in [Section 3](#). The simulation results of the proposed controller, compared with other techniques, are provided in [Section 4](#). The conclusion and open problems are given in [Section 5](#).

## **2. 6-DOF Quadrotor Model**

### *2.1. The Quadrotor Description*

The drone used in this work is a nano quadrotor depicted in [Figure 1](#). This machine is a rigid body equipped with four rotors. The movement of the quadrotor is controlled by adjusting the speeds of the rotors. The yaw movement is obtained by creating a difference in term of speed between two rotors in opposite direction. Effectively, between the rotors (2,4) and (1,3). The quadrotor vertical movement is obtained by decreasing or increasing the total rotor speeds. The forward motion is obtained by changing the (1 and 3) propeller's speed. The lateral motion is obtained by changing (2 and 4) propeller's speed. Therefore, the body is inherently unstable; its mechanical system is strongly coupled and under-actuated. Besides, in this paper the quadrotor dynamic model is obtained by using some assumptions as follows [38]:

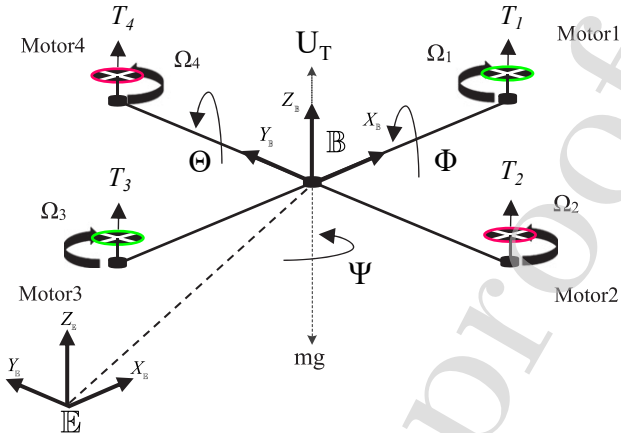


Figure 1: The quadrotor configuration.

**Assumption 1.** *The ground influence is neglected.*

**Assumption 2.** *The vehicle structure and the blades are rigid.*

**Assumption 3.** *The structure of the vehicle body is symmetrical.*

**Assumption 4.** *The torques ( $\tau_\Phi$ ,  $\tau_\Theta$ ,  $\tau_\Psi$ ) and thrust  $U_T$ , produced by the speeds of the rotors, are proportional to the square of rotational speeds of the rotors.*

## 2.2. Quadrotor Kinematics

The quadrotor is characterized by the body frame  $\mathbb{B} = \{O_{\mathbb{B}}, X_{\mathbb{B}}, Y_{\mathbb{B}}, Z_{\mathbb{B}}\}$ . The viewed inertial frame  $\mathbb{E} = \{O_{\mathbb{E}}, X_{\mathbb{E}}, Y_{\mathbb{E}}, Z_{\mathbb{E}}\}$  is fixed with respect to the ground. The quadrotor absolute position (Frame  $\mathbb{E}$ ) is represented by  $\chi = [X \ Y \ Z]^T$  and the Euler angles (i.e., roll, pitch, and yaw angles) is represented by  $\Upsilon = [\Phi \ \Theta \ \Psi]^T$ . The rotation of the quadrotor is described by using these angles with respect to the fixed frame. The roll and pitch angles, which are respectively symbolized by  $\Phi$  and  $\Theta$  are limited between  $-\frac{\pi}{2}$  and  $\frac{\pi}{2}$ , while the angle of yaw  $\Psi$  is limited between  $-\pi$  and  $\pi$ . The rotation matrix  $R_{\mathbb{B}}$  is used to determine the helicopter orientation  $R_{\mathbb{E}}$ :  $\mathbb{B} \longmapsto \mathbb{E}$ , where  $R_{\mathbb{B}}$  is the orthonormal

matrix, their expression is given by [21]:

$$R_{\mathbb{B}} = \begin{bmatrix} C_{\Psi}C_{\Theta} & S_{\Theta}S_{\Phi}C_{\Psi} - S_{\Psi}C_{\Phi} & C_{\Phi}C_{\Psi}S_{\Theta} + S_{\Phi}S_{\Psi} \\ C_{\Theta}S_{\Psi} & S_{\Phi}S_{\Psi}S_{\Theta} + C_{\Phi}S_{\Psi} & C_{\Phi}S_{\Psi}S_{\Theta} - S_{\Phi}C_{\Psi} \\ -S_{\Theta} & S_{\Phi}C_{\Theta} & C_{\Phi}C_{\Theta} \end{bmatrix} \quad (1)$$

with  $C_{\hbar} = \cos(\hbar)$  and  $S_{\hbar} = \sin(\hbar)$ , for  $\hbar = \Phi, \Theta$ , or  $\Psi$ . The translational kinematic can be obtained by the matrix  $R_{\mathbb{B}}$ .

$$N_{\mathbb{E}} = R_{\mathbb{B}}N_{\mathbb{B}} \quad (2)$$

where  $N_{\mathbb{E}}$  and  $N_{\mathbb{B}}$  represent respectively the linear velocity in the fixed frame and the linear velocity in the body frame. The vectors  $N_{\mathbb{E}} = [N_u \ N_v \ N_w]^T$  (Frame  $\mathbb{E}$ ) and  $\Omega = [\Omega_p \ \Omega_q \ \Omega_r]^T$  (frame  $\mathbb{B}$ ) respectively denote the linear and the angular velocities. The relationship, between the angular velocities  $(\Omega_p, \Omega_q, \Omega_r)$  and the time derivative of the  $(\Phi, \Theta, \Psi)$ , is given as [39]:

$$\dot{\Upsilon} = M_{\Upsilon}^{-1}\Omega \quad (3)$$

$$\begin{bmatrix} \dot{\Phi} \\ \dot{\Theta} \\ \dot{\Psi} \end{bmatrix} = \underbrace{\begin{bmatrix} 1 & \tan\Theta \sin\Phi & \tan\Theta \cos\Phi \\ 0 & \cos\Phi & -\sin\Phi \\ 0 & \sec\Theta \sin\Phi & \sec\Theta \cos\Phi \end{bmatrix}}_{M_{\Upsilon}^{-1}} \begin{bmatrix} \Omega_p \\ \Omega_q \\ \Omega_r \end{bmatrix} \quad (4)$$

This relationship describes the rotational kinematics of the vehicle.

### 2.3. The Quadrotor Dynamic

The quadrotor dynamics can be formulated by the Newton-Euler and the Lagrange-Euler methods. Based on the works developed in Refs. [21, 22, 40, 41], the quadrotor dynamic is obtained.

#### 2.3.1. Position Equations Via Lagrange-Euler Formalism

Using the Lagrange-Euler formalism to find the quadrotor position motion equations, this method is based on the potential and kinetic energy concept. However, the vehicle position dynamic can be expressed as follows:

$$f_{\chi} = \frac{d}{dt} \left( \frac{\partial LE}{\partial \dot{\chi}_i} \right) - \frac{\partial LE}{\partial \chi_i} \quad (5)$$

$$LE(\chi, \dot{\chi}) = E_T - E_U \quad (6)$$

$LE$  denotes the Lagrangian of the quadrotor position model,  $E_T = \frac{m}{2} \dot{\chi}^T \dot{\chi}$  represents the translational kinetic energy,  $E_U = mgZ$  represents the total potential energy, the term  $Z$  denotes the altitude of the vehicle,  $m$  represents the total mass,  $g$  is the acceleration due to gravity,  $f_\chi = R_{\mathbb{B}} \epsilon_3 U_T + d_\chi$  is the translational forces and the external disturbances,  $\epsilon_3 = [0 \ 0 \ 1]^T$ , and  $d_\chi = [d_1 \ d_2 \ d_3]^T$  is the aerodynamic force vector and the external disturbance. The expression of  $d_\chi$  is,

$$\begin{cases} d_1 = d_X - K_X \dot{X}/m \\ d_2 = d_Y - K_Y \dot{Y}/m \\ d_3 = d_Z - K_Z \dot{Z}/m \end{cases} \quad (7)$$

The translational equations can be expressed as:

$$m\ddot{\chi} + mge_3 = f_\chi \quad (8)$$

Hence, the acceleration of the  $\chi$  can be written in Eq. (9).

$$\begin{aligned} \ddot{X} &= -\frac{K_X}{m} \dot{X} + d_X + \frac{1}{m} (\sin \Theta \cos \Psi \cos \Phi + \sin \Psi \sin \Phi) U_T \\ \ddot{Y} &= -\frac{K_Y}{m} \dot{Y} + d_Y + \frac{1}{m} (\sin \Theta \sin \Psi \cos \Phi - \cos \Psi \sin \Phi) U_T \\ \ddot{Z} &= -\frac{K_Z}{m} \dot{Z} + d_Z - g + \frac{1}{m} (\cos \Theta \cos \Phi) U_T \end{aligned} \quad (9)$$

### 2.3.2. Attitude Equations Via Newton-Euler Method

The rotational dynamics can be written by using the Newton-Euler equation.

$$J_{\mathbb{B}} \dot{\Omega} = -\Omega^T \times J_{\mathbb{B}} \Omega + \tau_b - \tau_c - \tau_a + \tau_Y \quad (10)$$

where  $J_{\mathbb{B}} = diag(J_{xx}, J_{yy}, J_{zz})$  denotes the symmetric positive matrix with  $J_{zz}$ ,  $J_{yy}$ , and  $J_{xx}$  represent the rotary inertia respect to the  $O_{\mathbb{B}}Z_{\mathbb{B}}$ ,  $O_{\mathbb{B}}Y_{\mathbb{B}}$ , and  $O_{\mathbb{B}}X_{\mathbb{B}}$  axes. The term  $\tau_b$  represents the moment generated by four rotors of the vehicle. The term  $\tau_c$  symbolizes the resultant torque produced by the gyroscopic effects, their expression is defined as:

$$\tau_c = \sum_{\hbar=1}^4 \Omega^T J_r \begin{bmatrix} 0 \\ 0 \\ (-1)^{\hbar+1} \Omega_{\hbar} \end{bmatrix} \quad (11)$$

and the notation  $\tau_a$  denotes the resultant of aerodynamic friction torque defined as:

$$\tau_a = \begin{bmatrix} K_\Phi & 0 & 0 \\ 0 & K_\Theta & 0 \\ 0 & 0 & K_\Psi \end{bmatrix} \|\Omega\|^2 \quad (12)$$

with  $J_r$  is the rotor inertia and  $(K_\Phi, K_\Theta, K_\Psi)$  are aerodynamic friction coefficients.  $\tau_\gamma$  is an additive disturbance on quadrotor's angular acceleration.

Therefore, the acceleration of the quadrotor rotational movement is given as:

$$\begin{aligned} \ddot{\Phi} &= \frac{1}{J_{xx}}(\dot{\Theta}\dot{\Psi}(J_{yy} - J_{zz}) - J_r\dot{\Theta}\varpi - K_\Phi\dot{\Phi}^2 + U_\Phi) + d_\Phi \\ \ddot{\Theta} &= \frac{1}{J_{yy}}(\dot{\Phi}\dot{\Psi}(J_{zz} - J_{xx}) + J_r\dot{\Phi}\varpi - K_\Theta\dot{\Theta}^2 + U_\Theta) + d_\Theta \\ \ddot{\Psi} &= \frac{1}{J_{zz}}(\dot{\Phi}\dot{\Theta}(J_{xx} - J_{yy}) - K_\Psi\dot{\Psi}^2 + U_\Psi) + d_\Psi \end{aligned} \quad (13)$$

where  $\varpi = \Omega_4 + \Omega_3 - \Omega_2 - \Omega_1$ .

The quadrotor rotors produce a total lift defined as:

$$U_T = \sum_{\hbar=1}^4 T_\hbar = b_d \sum_{\hbar=1}^4 \Omega_\hbar^2 (\hbar = 1, 2, 3, 4) \quad (14)$$

whither  $b_d$  is a positive parameter and  $\Omega_\hbar$  denotes the angular rotor  $\hbar$  speed.

The control torque  $\tau_b$  developed by the quadrotor rotors (Frame  $\mathbb{B}$ ) is defined as:

$$\tau_b = \begin{bmatrix} U_\Phi \\ U_\Theta \\ U_\Psi \end{bmatrix} = \begin{bmatrix} \ell_d(T_4 - T_2) \\ \ell_d(T_3 - T_1) \\ c_d(\Omega_1^2 - \Omega_2^2 + \Omega_3^2 - \Omega_4^2) \end{bmatrix} \quad (15)$$

$c_d$  represents the drag coefficient and  $\ell_d$  is a positive parameter. The quadrotor equations are defined as:

$$\dot{\mathcal{Z}} = f(\mathcal{Z}) + g(\mathcal{Z})U + d_h (h = \Phi, \Theta, \Psi, X, Y, Z) \quad (16)$$

where  $\mathcal{Z} = [\Phi, \dot{\Phi}, \Theta, \dot{\Theta}, \Psi, \dot{\Psi}, X, \dot{X}, Y, \dot{Y}, Z, \dot{Z}] \in \mathbb{R}^{12}$  represents the state variables,  $f(\mathcal{Z})$  and  $g(\mathcal{Z})$  are nonlinear functions. [Equation 16](#) can be expressed

as:

$$\left\{ \begin{array}{l} \dot{\mathcal{X}}_1 = \mathcal{X}_2 \\ \dot{\mathcal{X}}_3 = \mathcal{X}_4 \\ \dot{\mathcal{X}}_5 = \mathcal{X}_6 \\ \dot{\mathcal{X}}_2 = \rho_{1\Phi}\mathcal{X}_4\mathcal{X}_6 + \rho_{2\Phi}\mathcal{X}_4 + \rho_{3\Phi}\mathcal{X}_2^2 + \rho_1U_\Phi + d_\Phi \\ \dot{\mathcal{X}}_4 = \rho_{1\Theta}\mathcal{X}_2\mathcal{X}_6 + \rho_{2\Theta}\mathcal{X}_2 + \rho_{3\Theta}\mathcal{X}_4^2 + \rho_2U_\Theta + d_\Theta \\ \dot{\mathcal{X}}_6 = \rho_{1\Psi}\mathcal{X}_2\mathcal{X}_4 + \rho_{2\Psi}\mathcal{X}_6^2 + \rho_3U_\Psi + d_\Psi \\ \dot{\mathcal{X}}_7 = \mathcal{X}_8 \\ \dot{\mathcal{X}}_9 = \mathcal{X}_{10} \\ \dot{\mathcal{X}}_{11} = \mathcal{X}_{12} \\ \dot{\mathcal{X}}_8 = \rho_X\mathcal{X}_8 + \frac{1}{m}(C_{\mathcal{X}_1}S_{\mathcal{X}_3}C_{\mathcal{X}_5} + S_{\mathcal{X}_1}S_{\mathcal{X}_5})U_T + d_X \\ \dot{\mathcal{X}}_{10} = \rho_Y\mathcal{X}_{10} + \frac{1}{m}(C_{\mathcal{X}_1}S_{\mathcal{X}_3}S_{\mathcal{X}_5} - S_{\mathcal{X}_1}C_{\mathcal{X}_5})U_T + d_Y \\ \dot{\mathcal{X}}_{12} = \rho_Z\mathcal{X}_{12} - g + \frac{1}{m}(C_{\mathcal{X}_1}C_{\mathcal{X}_3})U_T + d_Z \end{array} \right. \quad (17)$$

with:  $\rho_{1\Phi} = \frac{(J_{yy}-J_{zz})}{J_{xx}}$ ,  $\rho_{2\Phi} = \frac{-\varpi J_r}{J_{xx}}$ ,  $\rho_{3\Phi} = \frac{-K_\Phi}{J_{xx}}$ ,  $\rho_{1\Theta} = \frac{(J_{zz}-J_{xx})}{J_{yy}}$ ,  $\rho_{2\Theta} = \frac{\varpi J_r}{J_{yy}}$ ,  $\rho_{3\Theta} = \frac{-K_\Theta}{J_{yy}}$ ,  $\rho_{1\Psi} = \frac{(J_{xx}-J_{yy})}{J_{zz}}$ ,  $\rho_{2\Psi} = \frac{-K_\Psi}{J_{zz}}$ ,  $\rho_X = \frac{-K_X}{m}$ ,  $\rho_Y = \frac{-K_Y}{m}$ ,  $\rho_Z = \frac{-K_Z}{m}$ ,  $\rho_1 = \frac{1}{J_{xx}}$ ,  $\rho_2 = \frac{1}{J_{yy}}$ , and  $\rho_3 = \frac{1}{J_{zz}}$ . The relationship between the rotor speeds and the control signals is given by [39]:

$$\begin{bmatrix} U_\Psi \\ U_\Theta \\ U_\Phi \\ U_T \end{bmatrix} = \begin{bmatrix} c_d & -c_d & c_d & -c_d \\ -\ell_d b_d & 0 & b_d \ell_d & 0 \\ 0 & -\ell_d b_d & 0 & b_d \ell_d \\ b_d & b_d & b_d & b_d \end{bmatrix} \begin{bmatrix} \Omega_1^2 \\ \Omega_2^2 \\ \Omega_3^2 \\ \Omega_4^2 \end{bmatrix} \quad (18)$$

#### 2.4. Problem Formulation

The purpose of this work is to design a robust controller, which generates the thrust magnitude  $U_T$  and the torque  $U_i(i = \Phi, \Theta, \Psi)$  to stabilize the vehicle and to follow the reference trajectory  $[\Phi_d \ \Theta_d \ \Psi_d \ X_d \ Y_d \ Z_d]^T$  in a finite-time. The quadrotor has six outputs  $[\mathcal{X}_1 \ \mathcal{X}_3 \ \mathcal{X}_5 \ \mathcal{X}_7 \ \mathcal{X}_9 \ \mathcal{X}_{11}]^T$  and four control inputs  $[U_T \ U_\Phi \ U_\Theta \ U_\Psi]^T$ . To simplify the design procedure of the control scheme, the

position's virtual control  $V = [V_X \ V_Y \ V_Z]^T$  is established in Eq. (19).

$$\begin{bmatrix} V_X \\ V_Y \\ V_Z \end{bmatrix} = \begin{bmatrix} (C_{\mathcal{X}_1} C_{\mathcal{X}_5} S_{\mathcal{X}_3} + S_{\mathcal{X}_5} S_{\mathcal{X}_1}) \frac{U_T}{m} \\ (C_{\mathcal{X}_1} S_{\mathcal{X}_3} S_{\mathcal{X}_5} - S_{\mathcal{X}_1} C_{\mathcal{X}_5}) \frac{U_T}{m} \\ (C_{\mathcal{X}_1} C_{\mathcal{X}_3}) \frac{U_T}{m} - g \end{bmatrix} \quad (19)$$

Hence, the desired Euler angles  $(\Phi_d, \Theta_d)$  and the total thrust  $U_T$  can be obtained as:

$$\begin{cases} U_T &= m\sqrt{V_X^2 + V_Y^2 + (V_Z + g)^2} \\ \Phi_d &= \arctan(C_{\Theta_d}(\frac{V_X S_{\Psi_d} - V_Y C_{\Psi_d}}{V_Z + g})) \\ \Theta_d &= \arctan(\frac{V_X C_{\Psi_d} + V_Y S_{\Psi_d}}{V_Z + g}) \end{cases} \quad (20)$$

The desired position trajectory and the desired attitude angles are referred to as  $[X_d, Y_d, Z_d]^T$  and  $[\Phi_d, \Theta_d, \Psi_d]^T$ , respectively. The tracking attitude Eq. (21) and position Eq. (22) errors are defined.

$$\begin{bmatrix} e_1 \\ e_3 \\ e_5 \end{bmatrix} = \begin{bmatrix} \mathcal{X}_1 - \Phi_d \\ \mathcal{X}_3 - \Theta_d \\ \mathcal{X}_5 - \Psi_d \end{bmatrix}, \quad \begin{bmatrix} e_2 \\ e_4 \\ e_6 \end{bmatrix} = \begin{bmatrix} \mathcal{X}_2 - \dot{\Phi}_d \\ \mathcal{X}_4 - \dot{\Theta}_d \\ \mathcal{X}_6 - \dot{\Psi}_d \end{bmatrix} \quad (21)$$

$$\begin{bmatrix} e_7 \\ e_9 \\ e_{11} \end{bmatrix} = \begin{bmatrix} \mathcal{X}_7 - X_d \\ \mathcal{X}_9 - Y_d \\ \mathcal{X}_{11} - Z_d \end{bmatrix}, \quad \begin{bmatrix} e_8 \\ e_{10} \\ e_{12} \end{bmatrix} = \begin{bmatrix} \mathcal{X}_8 - \dot{X}_d \\ \mathcal{X}_{10} - \dot{Y}_d \\ \mathcal{X}_{12} - \dot{Z}_d \end{bmatrix} \quad (22)$$

### 3. Controller Design Methodology for Quadrotor UAV

In this part, we shall present a new controller for the attitude and position subsystems in the presence of disturbances and parametric uncertainties. The controller aim is to track the reference of the position trajectory and to stabilize the attitude subject to wind gust and unknown additive disturbances. A new robust ANFTSMC is adopted for the outer and inner loops as indicated in Figure 2. The proposed controller is not only able to achieve null steady-state error tracking, to handle the complex disturbances and to establish faster convergence rate, but it is also able to guesstimate the unknown upper bounds of the uncertainties. From Figure 2, it can be seen that the control scheme

composed of two loops: the inner loop (Attitude) and the outer-loop (Position). The inner loop is based on the nonlinear robust ANFTSMC that is applied to perform the quadrotor attitude stabilization. This loop gives the yawing, pitching, and rolling torques to control the angular and the velocity of the rotational subsystem. While the outer loop consists of the RANFTSMC that is used to obtain a robust path tracking in short time. This loop generates the reference angles ( $\Phi_d, \Theta_d$ ) and the total thrust  $U_T$ . The proposed control improves the tracking performances of the path reference and increases the robustness of the quadrotor's control system against the external perturbations caused by the wind gust compared with the backstepping sliding mode, integral backstepping sliding mode, and feedback linearization control methods.

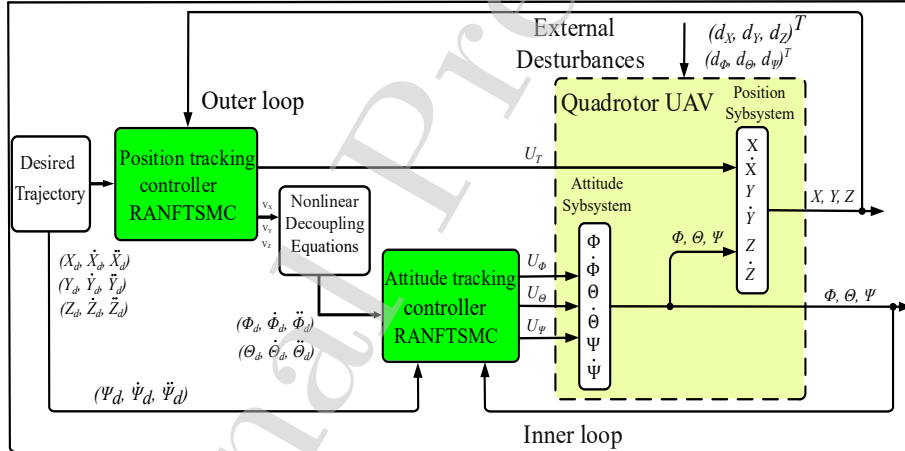


Figure 2: The general control scheme of the quadrotor.

### 3.1. Design of Path Following Controller for Quadrotor Position Based on NFTSMC Method

In this section, we shall present the design procedure of the virtual control input  $V_j (j = X, Y, Z)$  for the position subsystem. This control ensures the convergence of the position tracking errors in finite-time to zero asymptotically. The quadrotor position and attitude subsystems are a type of second-order nonlinear systems. However, The outer loop subsystem subjected to the uncertainties and

disturbances can be expressed as:

$$\begin{aligned}\dot{\mathcal{X}}_i &= \mathcal{X}_{i+1} \quad (i = 7, 9, 11) \\ \dot{\mathcal{X}}_{i+1} &= \mathcal{F}(\mathcal{P}) + \Delta\mathcal{P}(\mathcal{X}) + d + \mathcal{G}(\mathcal{X})V \\ \mathcal{Y}_i &= \mathcal{X}_i\end{aligned}\tag{23}$$

$$|D_k(\mathcal{X})| = |(\Delta\mathcal{P}(\mathcal{X}) + d)| \leq \delta_k \tag{24}$$

where  $\delta_k$  is the upper limit of uncertainty and disturbance. The expression of  $\delta_k$  can be given as [42–44]:

$$\delta_k = a_{0n} + a_{1n}|e_n| + a_{2n}|e_{n+1}| \quad (n = 7, 9, 11) \tag{25}$$

where  $a_{0n}$ ,  $a_{1n}$ , and  $a_{2n}$  are non-zero positive numbers.

Let's introduce the sliding surfaces of the position subsystem as [42, 45]:

$$\begin{aligned}\sigma_7 &= e_7 + b_7|e_7|^{\alpha_7}sign(e_7) + b_8|e_8|^{\beta_7}sign(e_8) \\ \sigma_9 &= e_9 + b_9|e_9|^{\alpha_9}sign(e_9) + b_{10}|e_{10}|^{\beta_9}sign(e_{10}) \\ \sigma_{11} &= e_{11} + b_{11}|e_{11}|^{\alpha_{11}}sign(e_{11}) + b_{12}|e_{12}|^{\beta_{11}}sign(e_{12})\end{aligned}\tag{26}$$

where  $b_n$  ( $n = 7, 9, 11$ ) and  $b_{n+1}$  are positive constants,  $1 < \beta_n < 2$  and  $\alpha_n > \beta_n$ .

The time derivative of sliding surfaces can be given as:

$$\begin{aligned}\dot{\sigma}_7 &= e_8 + \alpha_7 b_7 |e_7|^{\alpha_7-1} e_8 + \beta_7 b_8 |e_8|^{\beta_7-1} (\rho_X \mathcal{X}_8 + V_X + d_X - \ddot{X}_d) \\ \dot{\sigma}_9 &= e_{10} + \alpha_9 b_9 |e_9|^{\alpha_9-1} e_{10} + \beta_9 b_{10} |e_{10}|^{\beta_9-1} (\rho_Y \mathcal{X}_{10} + V_Y + d_Y - \ddot{Y}_d) \\ \dot{\sigma}_{11} &= e_{12} + \alpha_{11} b_{11} |e_{11}|^{\alpha_{11}-1} e_{12} + \beta_{11} b_{12} |e_{12}|^{\beta_{11}-1} (\rho_Z \mathcal{X}_{12} + V_Z + d_Z - \ddot{Z}_d)\end{aligned}\tag{27}$$

By setting  $\dot{\sigma}_n = 0$ , the equivalent control laws are given by:

$$\begin{aligned}V_{eqX} &= -(\rho_X \mathcal{X}_8 - \ddot{X}_d) - \frac{1}{\beta_7 b_8} |e_8|^{2-\beta_7} (1 + \alpha_7 b_7 |e_7|^{\alpha_7-1}) sign(e_8) \\ V_{eqY} &= -(\rho_Y \mathcal{X}_{10} - \ddot{Y}_d) - \frac{1}{\beta_9 b_{10}} |e_{10}|^{2-\beta_9} (1 + \alpha_9 b_9 |e_9|^{\alpha_9-1}) sign(e_{10}) \\ V_{eqZ} &= -(\rho_Z \mathcal{X}_{12} - \ddot{Z}_d) - \frac{1}{\beta_{11} b_{12}} |e_{12}|^{2-\beta_{11}} (1 + \alpha_{11} b_{11} |e_{11}|^{\alpha_{11}-1}) sign(e_{12})\end{aligned}\tag{28}$$

In order to reject the external factors and achieve the robustness against their influences of the position subsystem, the switching control law  $u_{sw} = -c\sigma - K sign(\sigma)$  is added to the equivalent control law, where  $c$  and  $K$  denote the

switching gains. The appropriate value of  $K$  is chosen as [46]:  $K = \delta_k + h$ , where  $h$  is a non-negative parameter and  $\delta_k$  represents the upper bound of the disturbances and uncertainties. We assume that the control signal contains only velocity and position measurements, so the switching controller is modified as follows:  $u_{sw} = -c\sigma - (a_{0n} + a_{1n}|e_n| + a_{2n}|e_{n+1}| + h)sign(\sigma)$ . Hence, switching control laws for quadrotor position are given by:

$$\begin{aligned}
 V_{swX} &= (-c_7\sigma_7 - K_7sign(\sigma_7)) \\
 &= (-c_7\sigma_7 - (\delta_7 + h_7)sign(\sigma_7)) \\
 &= (-c_7\sigma_7 - (a_{07} + a_{17}|e_7| + a_{27}|e_8| + h_7)sign(\sigma_7)) \\
 V_{swY} &= (-c_9\sigma_9 - K_9sign(\sigma_9)) \\
 &= (-c_9\sigma_9 - (\delta_9 + h_9)sign(\sigma_9)) \\
 &= (-c_9\sigma_9 - (a_{09} + a_{19}|e_9| + a_{29}|e_{10}| + h_9)sign(\sigma_9)) \\
 V_{swZ} &= (-c_{11}\sigma_{11} - K_{11}sign(\sigma_{11})) \\
 &= (-c_{11}\sigma_{11} - (\delta_{11} + h_{11})sign(\sigma_{11})) \\
 &= (-c_{11}\sigma_{11} - (a_{011} + a_{111}|e_{11}| + a_{211}|e_{12}| + h_{11})sign(\sigma_{11}))
 \end{aligned} \tag{29}$$

where  $h_n$  and  $c_n$  are positive constants. Therefore, the position control virtual laws are designed as:

$$\begin{aligned}
 V_X &= V_{swX} + V_{eqX} \\
 &= (-c_7\sigma_7 - (a_{07} + a_{17}|e_7| + a_{27}|e_8| + h_7)sign(\sigma_7) - \rho_X \mathcal{X}_8) \\
 &\quad + \ddot{X}_d - \frac{1}{\beta_7 b_8} |e_8|^{2-\beta_7} (1 + \alpha_7 b_7 |e_7|^{\alpha_7-1}) sign(e_8)
 \end{aligned} \tag{30}$$

$$\begin{aligned}
 V_Y &= V_{swY} + V_{eqY} \\
 &= (-c_9\sigma_9 - (a_{09} + a_{19}|e_9| + a_{29}|e_{10}| + h_9)sign(\sigma_9) - \rho_Y \mathcal{X}_{10}) \\
 &\quad + \dot{Y}_d - \frac{1}{\beta_9 b_{10}} |e_{10}|^{2-\beta_9} (1 + \alpha_9 b_9 |e_9|^{\alpha_9-1}) sign(e_{10})
 \end{aligned} \tag{31}$$

$$\begin{aligned}
 V_Z &= V_{swZ} + V_{eqZ} \\
 &= (-c_{11}\sigma_{11} - (a_{011} + a_{111}|e_{11}| + a_{211}|e_{12}| + h_{11})sign(\sigma_{11}) - \rho_Z \mathcal{X}_{12}) \\
 &\quad + \ddot{Z}_d - \frac{1}{\beta_{11} b_{12}} |e_{12}|^{2-\beta_{11}} (1 + \alpha_{11} b_{11} |e_{11}|^{\alpha_{11}-1}) sign(e_{12})
 \end{aligned} \tag{32}$$

**Theorem 1.** Considering the  $X$ -subsystem (9) and the surface (26), if the control law designed as (30), then the state variables of the  $X$ -subsystem converge to  $\sigma_7(t)$  in a finite time  $t_r$ . Furthermore, the tracking error variables can converge to zero in finite time.

**Proof.** In order to prove *Theorem 1*, the Lyapunov function candidate of the  $X$ -subsystem is considered as:

$$V_7 = \frac{1}{2}\sigma_7^2 \quad (33)$$

The time derivative of  $V_7$  is,

$$\dot{V}_7 = \dot{\sigma}_7\sigma_7 = \sigma_7(e_8 + \alpha_7 b_7 |e_7|^{\alpha_7-1} e_8 + \beta_7 b_8 |e_8|^{\beta_7-1} \dot{e}_8) \quad (34)$$

By substituting Eq. (22) and Eq. (30) into Eq. (34), the dynamic of  $V_7$  can be written as:

$$\begin{aligned} \dot{V}_7 &= \beta_7 b_8 |e_8|^{\beta_7-1} (D_7 \sigma_7 - c_7 \sigma_7^2 - (\delta_7 + h_7) |\sigma_7|) \\ &\leq \beta_7 b_8 |e_8|^{\beta_7-1} (|(D_7)| |\sigma_7| - c_7 \sigma_7^2 - (\delta_7 + h_7) |\sigma_7|) \\ &= \beta_7 b_8 |e_8|^{\beta_7-1} (|(D_7) - \delta_7| |\sigma_7| - c_7 \sigma_7^2 - h_7 |\sigma_7|) \end{aligned} \quad (35)$$

Using Eq. (24), we can get,

$$\dot{V}_7 \leq \beta_7 b_8 |e_8|^{\beta_7-1} (-c_7 \sigma_7^2 - h_7 |\sigma_7|) \leq 0 \quad (36)$$

From Eq. (35), the condition of stability is guaranteed.

The state variables of system converge to  $\sigma_7(t) = 0$  asymptotically. In order to demonstrate that this convergence, Eq. (36) can be rewritten as:

$$\dot{V}_7 \leq \frac{dV_7}{dt} \leq -2\beta_7 b_8 c_7 |e_8|^{\beta_7-1} V_7 - \sqrt{2}\beta_7 b_8 h_7 |e_8|^{\beta_7-1} V_7^{1/2} \quad (37)$$

By defining  $\hbar_1 = -2\beta_7 b_8 c_7 |e_8|^{\beta_7-1}$  and  $\hbar_2 = -\sqrt{2}\beta_7 b_8 h_7 |e_8|^{\beta_7-1}$ , it results:

$$\frac{dV_7}{dt} \leq -\hbar_1 V_7 - \hbar_2 V_7^{1/2} \quad (38)$$

After some calculation, we get,

$$dt \leq \frac{-dV_7}{\hbar_1 V_7 + \hbar_2 V_7^{1/2}} = \frac{-dV_7^{1/2}}{\hbar_1 V_7 + \hbar_2} \quad (39)$$

Now, integratting Eq. (39) from  $t_0$  to  $t_r$ , one can obtain,

$$t_r \leq t_0 + \frac{2}{\hbar_1} \ln\left(\frac{\hbar_1 V_7(t_0)^{1/2} + \hbar_2}{\hbar_2}\right) \quad (40)$$

This complete the proof above.

### 3.2. Design of Path Following Controller for Quadrotor Position Based on RANFTSMC Method

The RANFTSMC approach is developed to estimate the unknown upper limits of disturbances that affected the position subsystem. Therefore, the control signals of the position are modified as:

$$\begin{aligned} V_X = & V_{swX} + V_{eqX} \\ = & (-c_7\sigma_7 - (\hat{a}_{07} + \hat{a}_{17}|e_7| + \hat{a}_{27}|e_8| + h_7)sign(\sigma_7) - \rho_X \mathcal{X}_8) \\ & + \ddot{X}_d - \frac{1}{\beta_7 b_8} |e_8|^{2-\beta_7} (1 + \alpha_7 b_7 |e_7|^{\alpha_7-1}) sign(e_8) \end{aligned} \quad (41)$$

$$\begin{aligned} V_Y = & V_{swY} + V_{eqY} \\ = & (-c_9\sigma_9 - (\hat{a}_{09} + \hat{a}_{19}|e_9| + \hat{a}_{29}|e_{10}| + h_9)sign(\sigma_9) - \rho_Y \mathcal{X}_{10}) \\ & + \ddot{Y}_d - \frac{1}{\beta_9 b_{10}} |e_{10}|^{2-\beta_9} (1 + \alpha_9 b_9 |e_9|^{\alpha_9-1}) sign(e_{10}) \end{aligned} \quad (42)$$

$$\begin{aligned} V_Z = & V_{swZ} + V_{eqZ} \\ = & (-c_{11}\sigma_{11} - (\hat{a}_{011} + \hat{a}_{111}|e_{11}| + \hat{a}_{211}|e_{12}| + h_{11})sign(\sigma_{11}) - \rho_Z \mathcal{X}_{12}) \\ & + \ddot{Z}_d - \frac{1}{\beta_{11} b_{12}} |e_{12}|^{2-\beta_{11}} (1 + \alpha_{11} b_{11} |e_{11}|^{\alpha_{11}-1}) sign(e_{12}) \end{aligned} \quad (43)$$

where  $\hat{a}_{0n}$ ,  $\hat{a}_{1n}$ , and  $\hat{a}_{2n}$  ( $n = 7, 9, 11$ ) are the estimates of  $a_{0n}$ ,  $a_{1n}$ , and  $a_{2n}$ , respectively. The parameters  $\hat{a}_{0n}$ ,  $\hat{a}_{1n}$ , and  $\hat{a}_{2n}$  are amended by the adaptive laws.

$$\dot{\hat{a}}_{07} = \mu_{07} |\sigma_7| \cdot |e_8|^{\beta_7-1}, \quad \dot{\hat{a}}_{09} = \mu_{09} |\sigma_9| \cdot |e_{10}|^{\beta_9-1}, \quad \text{and} \quad \dot{\hat{a}}_{011} = \mu_{011} |\sigma_{11}| \cdot |e_{12}|^{\beta_{11}-1} \quad (44)$$

$$\begin{aligned} \dot{\hat{a}}_{17} = & \mu_{17} |\sigma_7| \cdot |e_7| \cdot |e_8|^{\beta_7-1}, \quad \dot{\hat{a}}_{19} = \mu_{19} |\sigma_9| \cdot |e_9| \cdot |e_{10}|^{\beta_9-1}, \\ \text{and} \quad \dot{\hat{a}}_{111} = & \mu_{111} |\sigma_{11}| \cdot |e_{11}| \cdot |e_{12}|^{\beta_{11}-1} \end{aligned} \quad (45)$$

$$\dot{\hat{a}}_{27} = \mu_{27} |\sigma_7| \cdot |e_8|^{\beta_7}, \quad \dot{\hat{a}}_{29} = \mu_{29} |\sigma_9| \cdot |e_{10}|^{\beta_9}, \quad \text{and} \quad \dot{\hat{a}}_{211} = \mu_{211} |\sigma_{11}| \cdot |e_{12}|^{\beta_{11}} \quad (46)$$

where  $\mu_{0i}$ ,  $\mu_{1i}$ , and  $\mu_{2i}$  ( $i = 7, 9, 11$ ) are non-zero positive constants.

**Theorem 2.** Considering the X-subsystem (9) with the designed controller (41) and the adaptive control laws (44)–(46), then the state variables of the X-subsystem converge to the sliding surface (26) in a finite time.

**Proof.** To determine the parameters  $(\hat{a}_{07}, \hat{a}_{17}, \hat{a}_{27})$  and prove the system stability, the Lyapunov approach is used. The Lyapunov function candidate of the  $X$ -subsystem is considered as follows:

$$V_7 = \frac{1}{2}\sigma_7^2 + \beta_7 b_8 \sum_{i=0}^2 \frac{1}{2\mu_{i7}} (\hat{a}_{i7} - a_{i7})^2 \quad (47)$$

The time derivative of Eq. (47) is,

$$\dot{V}_7 = \dot{\sigma}_7 \sigma_7 + \beta_7 b_8 \sum_{i=0}^2 \frac{1}{\mu_{i7}} (\hat{a}_{i7} - a_{i7}) \dot{\hat{a}}_{i7} \quad (48)$$

From Eq. (27), we can get,

$$\dot{V}_7 = \sigma_7 (e_8 + \alpha_7 b_7 |e_7|^{\alpha_7-1} e_8 + \beta_7 b_8 |e_8|^{\beta_7-1} \dot{e}_8) + \beta_7 b_8 \sum_{i=0}^2 \frac{1}{\mu_{i7}} (\hat{a}_{i7} - a_{i7}) \dot{\hat{a}}_{i7} \quad (49)$$

From Eqs. (22) and (41), the dynamic of  $V_7$  is given by:

$$\begin{aligned} \dot{V}_7 = & \beta_7 b_8 |e_8|^{\beta_7-1} (D_7 \sigma_7 - c_7 \sigma_7^2 - (\hat{a}_{07} + \hat{a}_{17} |e_7| + \hat{a}_{27} |e_8| + h_7) |\sigma_7|) \\ & + \beta_7 b_8 \sum_{i=0}^2 \frac{1}{\mu_{i7}} (\hat{a}_{i7} - a_{i7}) \dot{\hat{a}}_{i7} \end{aligned} \quad (50)$$

Using Eqs. (44)–(46), we can get,

$$\dot{V}_7 = \beta_7 b_8 |e_8|^{\beta_7-1} (D_7 \sigma_7 - h_7 |\sigma_7| - c_7 \sigma_7^2 - (\hat{a}_{07} + \hat{a}_{17} |e_7| + \hat{a}_{27} |e_8|) |\sigma_7|) \quad (51)$$

From Eq. (24), we obtain,

$$\begin{aligned} \dot{V}_7 \leq & \beta_7 b_8 |e_8|^{\beta_7-1} (|(D_7| |\sigma_7| - h_7 |\sigma_7|) - c_7 \sigma_7^2 - (a_{07} + a_{17} |e_7| a_{27} |e_8|) |\sigma_7|) \\ \leq & \beta_7 b_8 |e_8|^{\beta_7-1} (-h_7 |\sigma_7| - c_7 \sigma_7^2) \\ \leq & 0 \end{aligned} \quad (52)$$

The Lyapunov equation  $\dot{V}_7 \leq 0$  can guarantee that position velocity errors will converge to zero in short finite-time.

**Theorem 3.** The controllers  $V_X$ ,  $V_Y$ , and  $V_Z$  applied to the investigated system (9) ensure the asymptotic stability of the translational subsystem.

**Proof.** Consider the Lyapunov function for the translational subsystem as follows:

$$\begin{aligned} V_T = & \frac{1}{2}\sigma_7^2 + \beta_7 b_8 \sum_{i=0}^2 \frac{1}{2\mu_{i7}} (\hat{a}_{i7} - a_{i7})^2 + \frac{1}{2}\sigma_9^2 + \beta_9 b_{10} \sum_{i=0}^2 \frac{1}{2\mu_{i9}} (\hat{a}_{i9} - a_{i9})^2 \\ & + \frac{1}{2}\sigma_{11}^2 + \beta_{11} b_{12} \sum_{i=0}^2 \frac{1}{2\mu_{i11}} (\hat{a}_{i11} - a_{i11})^2 \end{aligned} \quad (53)$$

The dynamic of  $V_T$  is,

$$\begin{aligned}\dot{V}_T = & \dot{\sigma}_7\sigma_7 + \beta_7 b_8 \sum_{i=0}^2 \frac{1}{\mu_{i7}} (\hat{a}_{i7} - a_{i7}) \dot{a}_{i7} + \beta_9 b_{10} \sum_{i=0}^2 \frac{1}{\mu_{i9}} (\hat{a}_{i9} - a_{i9}) \dot{a}_{i9} \\ & + \dot{\sigma}_9\sigma_9 + \dot{\sigma}_{11}\sigma_{11} + \beta_{11} b_{11} \sum_{i=0}^2 \frac{1}{\mu_{i11}} (\hat{a}_{i11} - a_{i11}) \dot{a}_{i11}\end{aligned}\quad (54)$$

From Eqs. (24), (27) and (41)–(46), we can obtain,

$$\begin{aligned}\dot{V}_T \leq & \beta_7 b_8 |e_8|^{\beta_7-1} (-h_7 |\sigma_7| - c_7 \sigma_7^2) + \beta_9 b_{10} |e_{10}|^{\beta_9-1} (-h_9 |\sigma_9| - c_9 \sigma_9^2) \\ & + \beta_{11} b_{12} |e_{12}|^{\beta_{11}-1} (-h_{11} |\sigma_{11}| - c_{11} \sigma_{11}^2) \\ \leq & 0\end{aligned}\quad (55)$$

From the above analysis, it is evident that the reaching condition of outer loop stability is guaranteed.

In this part, a robust RANFTSMC law for the position control is provided. The outer-loop stability is guaranteed by using the Lyapunov analysis. Similarly, a robust ANFTSMC law for the attitude loop is presented in the following subsection.

### 3.3. Design of Path Following Controller for Quadrotor Attitude Based on RANFTSMC Method

In this part, we shall present a RANFTSM controller for the disturbed attitude. The control law generated by this loop ensures the stability of the attitude in the closed-loop. The controller proposed in this work for the quadrotor attitude allows that the roll, pitch and yaw states variables ( $\mathcal{X}_1, \mathcal{X}_3, \mathcal{X}_5$ ) converge to the desired values ( $\Phi_d, \Theta_d, \Psi_d$ ) in a short time. Therefore, the same control procedure presented in the previous subsection 3.2 for the quadrotor position can be conducted to design the quadrotor attitude. The corresponding RANFTSMC surfaces for the quadrotor attitude are chosen as:

$$\begin{aligned}\sigma_1 = & e_1 + b_1 |e_1|^{\alpha_1} sign(e_1) + b_2 |e_2|^{\beta_1} sign(e_2) \\ \sigma_3 = & e_3 + b_3 |e_3|^{\alpha_3} sign(e_3) + b_4 |e_4|^{\beta_3} sign(e_4) \\ \sigma_5 = & e_5 + b_5 |e_5|^{\alpha_5} sign(e_5) + b_6 |e_6|^{\beta_5} sign(e_6)\end{aligned}\quad (56)$$

where  $b_j (j = 1, 3, 5)$  and  $b_{j+1}$  are positive constants,  $1 < \beta_j < 2$  and  $\alpha_j > \beta_j$ . The corresponding RANFTSMC controllers for the inner loop are designed as:

$$\begin{aligned} U_\Phi &= U_{sw\Phi} + U_{eq\Phi} \\ &= \rho_1[-c_1\sigma_1 - (\hat{a}_{01} + \hat{a}_{11}|e_1| + \hat{a}_{21}|e_2| + h_1)sign(\sigma_1) - (\rho_{1\Phi}\mathcal{X}_6\mathcal{X}_4 + \rho_{2\Phi}\mathcal{X}_4) \\ &\quad - \rho_{3\Phi}\mathcal{X}_2^2 + \ddot{\Phi}_d - \frac{1}{\beta_1 b_2}|e_2|^{2-\beta_1}(1 + \alpha_1 b_1|e_1|^{\alpha_1-1})sign(e_2)] \end{aligned} \quad (57)$$

$$\begin{aligned} U_\Theta &= U_{sw\Theta} + U_{eq\Theta} \\ &= \rho_2[-c_3\sigma_3 - (\hat{a}_{03} + \hat{a}_{13}|e_3| + \hat{a}_{23}|e_4| + h_3)sign(\sigma_3) - (\rho_{1\Theta}\mathcal{X}_6\mathcal{X}_2 + \rho_{2\Theta}\mathcal{X}_2) \\ &\quad - \rho_{3\Theta}\mathcal{X}_4^2 + \ddot{\Theta}_d - \frac{1}{\beta_3 b_4}|e_4|^{2-\beta_3}(1 + \alpha_3 b_3|e_3|^{\alpha_3-1})sign(e_4)] \end{aligned} \quad (58)$$

$$\begin{aligned} U_\Psi &= U_{sw\Psi} + U_{eq\Psi} \\ &= \rho_3[-c_5\sigma_5 - (\hat{a}_{05} + \hat{a}_{15}|e_5| + \hat{a}_{25}|e_6| + h_5)sign(\sigma_5) - (\rho_{1\Psi}\mathcal{X}_4\mathcal{X}_2 + \rho_{2\Psi}\mathcal{X}_6^2) \\ &\quad + \ddot{\Psi}_d - \frac{1}{\beta_5 b_6}|e_6|^{2-\beta_5}(1 + \alpha_5 b_5|e_5|^{\alpha_5-1})sign(e_6)] \end{aligned} \quad (59)$$

where  $\hat{a}_{0j}$ ,  $\hat{a}_{1j}$ , and  $\hat{a}_{2j}$  ( $j = 1, 3, 5$ ) are the estimates of  $a_{0j}$ ,  $a_{1j}$ , and  $a_{2j}$ , respectively.  $c_j (j = 1, 3, 5)$  and  $h_j$  are non-negative parameters. The adaptive laws of the attitude subsystem are given by:

$$\dot{\hat{a}}_{01} = \mu_{01}|\sigma_1|.|e_2|^{\beta_1-1}, \quad \dot{\hat{a}}_{03} = \mu_{03}|\sigma_3|.|e_4|^{\beta_3-1}, \quad \text{and} \quad \dot{\hat{a}}_{05} = \mu_{05}|\sigma_5|.|e_6|^{\beta_5-1} \quad (60)$$

$$\begin{aligned} \dot{\hat{a}}_{11} &= \mu_{11}|\sigma_1|.|e_1|.|e_2|^{\beta_1-1}, \quad \dot{\hat{a}}_{13} = \mu_{13}|\sigma_3|.|e_3|.|e_4|^{\beta_3-1}, \\ &\quad \text{and} \quad \dot{\hat{a}}_{15} = \mu_{15}|\sigma_5|.|e_5|.|e_6|^{\beta_5-1} \end{aligned} \quad (61)$$

$$\dot{\hat{a}}_{21} = \mu_{21}|\sigma_1|.|e_2|^{\beta_1}, \quad \dot{\hat{a}}_{23} = \mu_{23}|\sigma_3|.|e_4|^{\beta_3}, \quad \text{and} \quad \dot{\hat{a}}_{25} = \mu_{25}|\sigma_5|.|e_6|^{\beta_5} \quad (62)$$

where  $\mu_{0j}$ ,  $\mu_{1j}$ , and  $\mu_{2j} (j = 1, 3, 5)$  are non-zero positive constants.

**Theorem 4.** *The controllers  $U_\Phi$ ,  $U_\Theta$ , and  $U_\Psi$  applied to the investigated system (13) ensure the asymptotic stability of the rotational subsystem.*

**Proof.** *The Lyapunov function candidate for the rotational subsystem is con-*

sidered as follows:

$$\begin{aligned} V_R = & \frac{1}{2}\sigma_1^2 + \beta_1 b_2 \sum_{i=0}^2 \frac{1}{2\mu_{i1}}(\hat{a}_{i1} - a_{i3})^2 + \frac{1}{2}\sigma_3^2 + \beta_3 b_4 \sum_{i=0}^2 \frac{1}{2\mu_{i3}}(\hat{a}_{i3} - a_{i3})^2 \\ & + \frac{1}{2}\sigma_5^2 + \beta_5 b_6 \sum_{i=0}^2 \frac{1}{2\mu_{i5}}(\hat{a}_{i5} - a_{i5})^2 \end{aligned} \quad (63)$$

The time-derivative of  $V_R$  is given by:

$$\begin{aligned} \dot{V}_R = & \dot{\sigma}_1 \sigma_1 + \beta_1 b_2 \sum_{i=0}^2 \frac{1}{\mu_{i1}}(\hat{a}_{i1} - a_{i1})\dot{a}_{i1} + \beta_3 b_4 \sum_{i=0}^2 \frac{1}{\mu_{i3}}(\hat{a}_{i3} - a_{i3})\dot{a}_{i3} \\ & + \dot{\sigma}_3 \sigma_3 + \dot{\sigma}_5 \sigma_5 + \beta_5 b_6 \sum_{i=0}^2 \frac{1}{\mu_{i5}}(\hat{a}_{i5} - a_{i5})\dot{a}_{i5} \end{aligned} \quad (64)$$

From Eqs. (24) and (57)–(62), we can obtain,

$$\begin{aligned} \dot{V}_R \leq & \beta_1 b_2 |e_2|^{\beta_1-1}(-h_1|\sigma_1| - c_1\sigma_1^2) + \beta_3 b_4 |e_4|^{\beta_3-1}(-h_3|\sigma_3| - c_3\sigma_3^2) \\ & + \beta_5 b_6 |e_6|^{\beta_5-1}(-h_5|\sigma_5| - c_5\sigma_5^2) \\ \leq & 0 \end{aligned} \quad (65)$$

From the above analysis, it is evident that the reaching condition of attitude loop stability is guaranteed.

**Theorem 5.** The ultimate control laws Eqs. (41)–(43) and (57)–(59) applied to the investigated system (17) and the adaptive laws are obtained via the RAN-FTSMC technique guarantees the overall closed-loop system stability.

**Proof.** The Lyapunov function for the quadrotor system is chosen as follows:

$$V_S = V_R + V_T \quad (66)$$

The time-derivative of  $V_S$  is given by:

$$\dot{V}_S = \dot{V}_R + \dot{V}_T \quad (67)$$

From Eqs. (55) and (65), we have,

$$\begin{aligned} \dot{V}_S \leq & \beta_1 b_2 |e_2|^{\beta_1-1}(-h_1|\sigma_1| - c_1\sigma_1^2) + \beta_3 b_4 |e_4|^{\beta_3-1}(-h_3|\sigma_3| - c_3\sigma_3^2) \\ & + \beta_5 b_6 |e_6|^{\beta_5-1}(-h_5|\sigma_5| - c_5\sigma_5^2) + \beta_7 b_8 |e_8|^{\beta_7-1}(-h_7|\sigma_7| - c_7\sigma_7^2) \\ & + \beta_9 b_{10} |e_{10}|^{\beta_9-1}(-h_9|\sigma_9| - c_9\sigma_9^2) + \beta_{11} b_{12} |e_{12}|^{\beta_{11}-1}(-h_{11}|\sigma_{11}| - c_{11}\sigma_{11}^2) \\ \leq & 0 \end{aligned} \quad (68)$$

The global stability of the rotational and translational tracking errors is proved according to the Lyapunov approach.

#### 4. Simulation Results

In this part, the efficiency of the proposed control strategy, based on RANFTSMC method for the path following problem, has been tested under different disturbances using numerical simulations. In order to show the improvement obtained by using the ANFTSMC approach, a comparative study with three other controllers is considered. The existing controllers presented in this work are the nonlinear backstepping sliding mode controller (BSMC) ([9, 10]), the feedback linearization (FL) technique [47], and the integral backstepping sliding mode controller (IBSMC) [39]. Table 1 summarizes the quadrotor physical parameters used in these simulations refer to [21]. The RANFTSMC parameters are shown in Table 2.

**Remark 1.** *These parameters need to be adjusted to reach the requirement of performance of the quadrotor system. For these reasons, The toolbox of optimization in MATLAB software is utilized to select the best values of the controller parameters in Simulation 1 (without disturbances), then we kept the same parameters for the rest of the proposed scenarios (see Ref. [48]).*

Moreover, to evaluate the proposed control strategy multiple scenarios are proposed.

**Remark 2.** *The simulations are performed on MATLAB software, which is fitted with a Lenovo computer comprising 3.4 GHz CPU with 8GB of RAM and a 466 GB SSD.*

Table 1: The parameters of a quadrotor.

Parameter	Value	Parameter	Value
$g$	9.81 $s^{-2}.m$	$K_Y$	5.5670e-4 $m^{-1}.s.N$
$m$	0.74 $kg$	$K_Z$	5.5670e-4 $m^{-1}.s.N$
$J_{xx}$	0.004 $kg.m^2$	$K_\Phi$	5.5670e-4 $rad^{-1}.s.N$
$J_{yy}$	0.004 $kg.m^2$	$K_\Theta$	5.5670e-4 $rad^{-1}.s.N$
$J_{zz}$	0.0084 $kg.m^2$	$K_\Psi$	5.5670e-4 $rad^{-1}.s.N$
$J_r$	2.8385e-5 $kg.m^2$	$b_d$	2.9842e-3 $N.s^2$
$K_X$	5.5670e-4 $m^{-1}.s.N$	$c_d$	3.2320e-2 $N.m.s^2$

Table 2: The design parameters of the RANFTSM controller.

Parameter	Value	Parameter	Value	Parameter	Value
$b_j$	8.7406	$b_{j+1}$	0.4838	$b_n$	0.03
$c_j$	11.7180	$\beta_j$	1.0885	$b_{n+1}$	0.8
$h_j$	0.5	$\mu_{0j}$	0.0118	$c_n$	1.21
$\mu_{1j}$	6.2942e-04	$\mu_{2j}$	0.01	$\beta_n$	5/3
$\alpha_j$	1.2	$\mu_{0n}$	0.5	$\mu_{1n}$	0.001
$\alpha_n$	2	$\mu_{2n}$	0.01	$h_n$	0.5

#### 4.1. Simulation 1

In this scenario, the quadrotor tracks a square reference trajectory without external perturbations. More specifically, the desired trajectory is given in Table 3.

Table 3: The desired square trajectory.

Variable	Value	Time(s)
$[X_d(m), Y_d(m), Z_d(m)]$	$[0.6, 0.6, 0.6]$	0
	$[0.3, 0.6, 0.6]$	10
	$[0.3, 0.3, 0.6]$	20
	$[0.6, 0.3, 0.6]$	30
	$[0.6, 0.6, 0.6]$	40
	$[0.6, 0.6, 0.0]$	50
$[\Psi_d(rad)]$	$[0.5]$	0
	$[0.0]$	50

Besides, the initial conditions of the vehicle in this case are null. The simulation results are illustrated in Figures 3–9 via the comparisons of FL, BSMC, and the proposed RANFTSMC. Figures 3 and 4 display the performance tracking of the quadrotor attitude and position. It can be observed that the yaw angle and position variables ( $\Psi, X, Y, Z$ ) are driven to their references more rapidly and more accurately. Moreover, the roll and pitch angles converge to zero (see Figure 4), that indicates the attitude subsystem is stable. Figure 5 display the performance of the control inputs of the quadrotor ( $U_T, \tau_\Phi, \tau_\Theta, \tau_\Psi$ ), as can be observed, the control signals are smooth and converge to their original values (**7.259, 0, 0, 0**), that proves the effectiveness of the RAFTSMC strategy. Indeed, the input system has better performances regarding this problem. The chattering problem is avoided by replacing the *sign()* function in the control laws by the *tanh(.)* function. Moreover, the attitude tracking errors and the position tracking errors are illustrated in Figures 6 and 7. Good tracking performances are achieved of the position ( $X, Y, Z$ ) using the ANFTSMC technique. The tracking errors of attitude are quickly converging to zero. The adaptive mechanism assures good tracking performances. However, it can be clearly seen, from both Figures 8 and 9 that the parameters estimated converge to constant values. Compared with the backstepping sliding mode and feedback

linearization control methods, these techniques can not provide good accuracy for tracking the desired yaw angle and desired position (see Figures 3 and 4). Then the performance of the tracking errors is not as good as the proposed RANTSMD method. Figures 3 and 4 show FL and BSMC techniques that ensure a damped response with large overshoot compared with the proposed controller.

#### 4.2. Simulation 2

The simulation is conducted with a circular trajectory defined as follows:

$$X_d = \frac{1}{2} \cos\left(\frac{\pi t}{20}\right)m, \quad Y_d = \frac{1}{2} \sin\left(\frac{\pi t}{20}\right)m, \quad Z_d = 2 - \frac{1}{2} \cos\left(\frac{\pi t}{20}\right)m, \quad \Psi_d = 0 \text{ rad} \quad (69)$$

The vehicle initial conditions are [0, 0, 0.5]rad and [0, 0, 0]m. In this simulation, the RANFTSMC proposed in this work is applied for the quadrotor subjected to the constant disturbances, their expressions are given by:

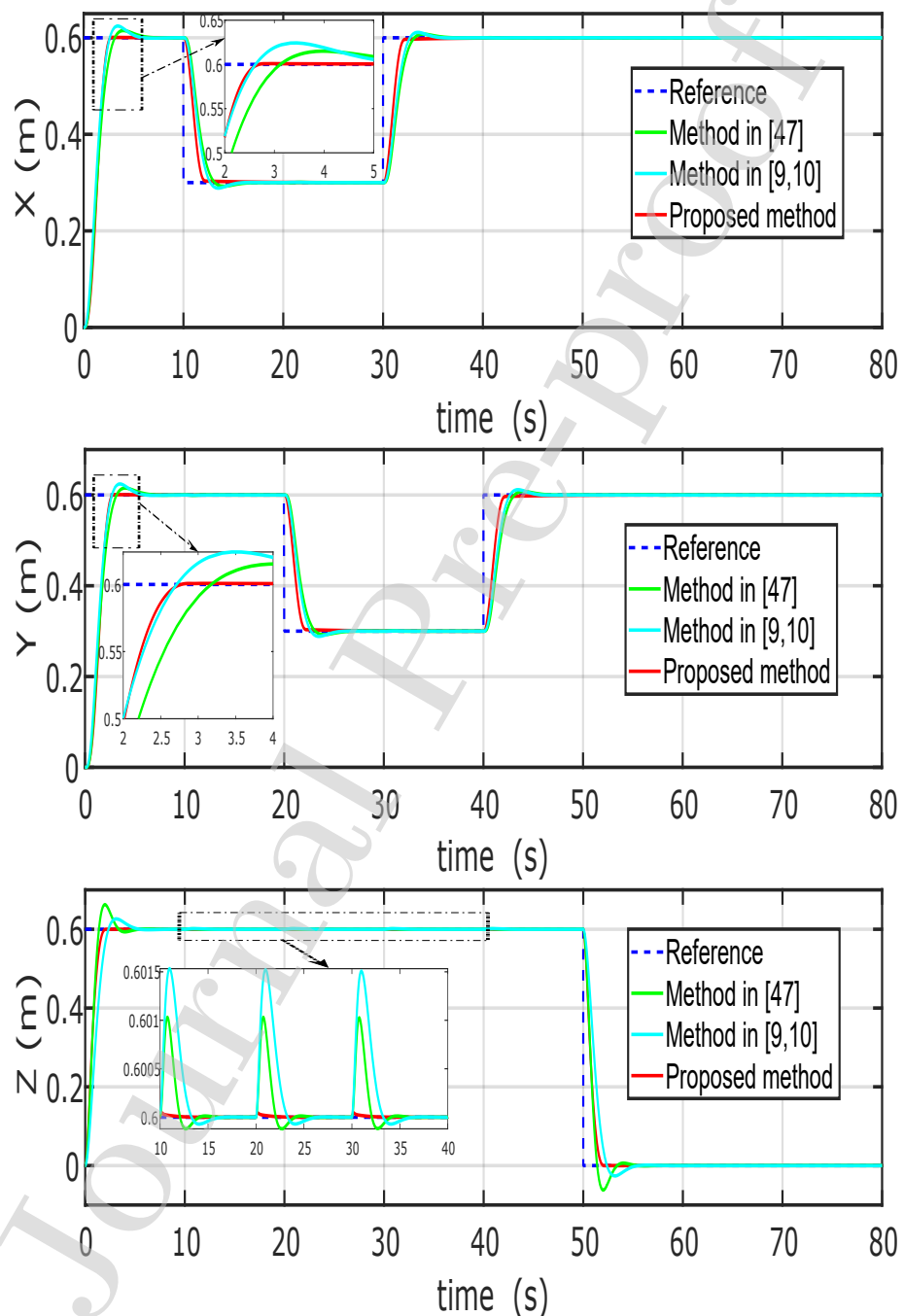
$$d_X = \begin{cases} 0 & m/s^2 t \in [0, 5) \\ 1 & m/s^2 [5, 40] \end{cases} \quad d_Y = \begin{cases} 0 & m/s^2 t \in [0, 15) \\ 1 & m/s^2 t \in [15, 40] \end{cases} \quad (70)$$

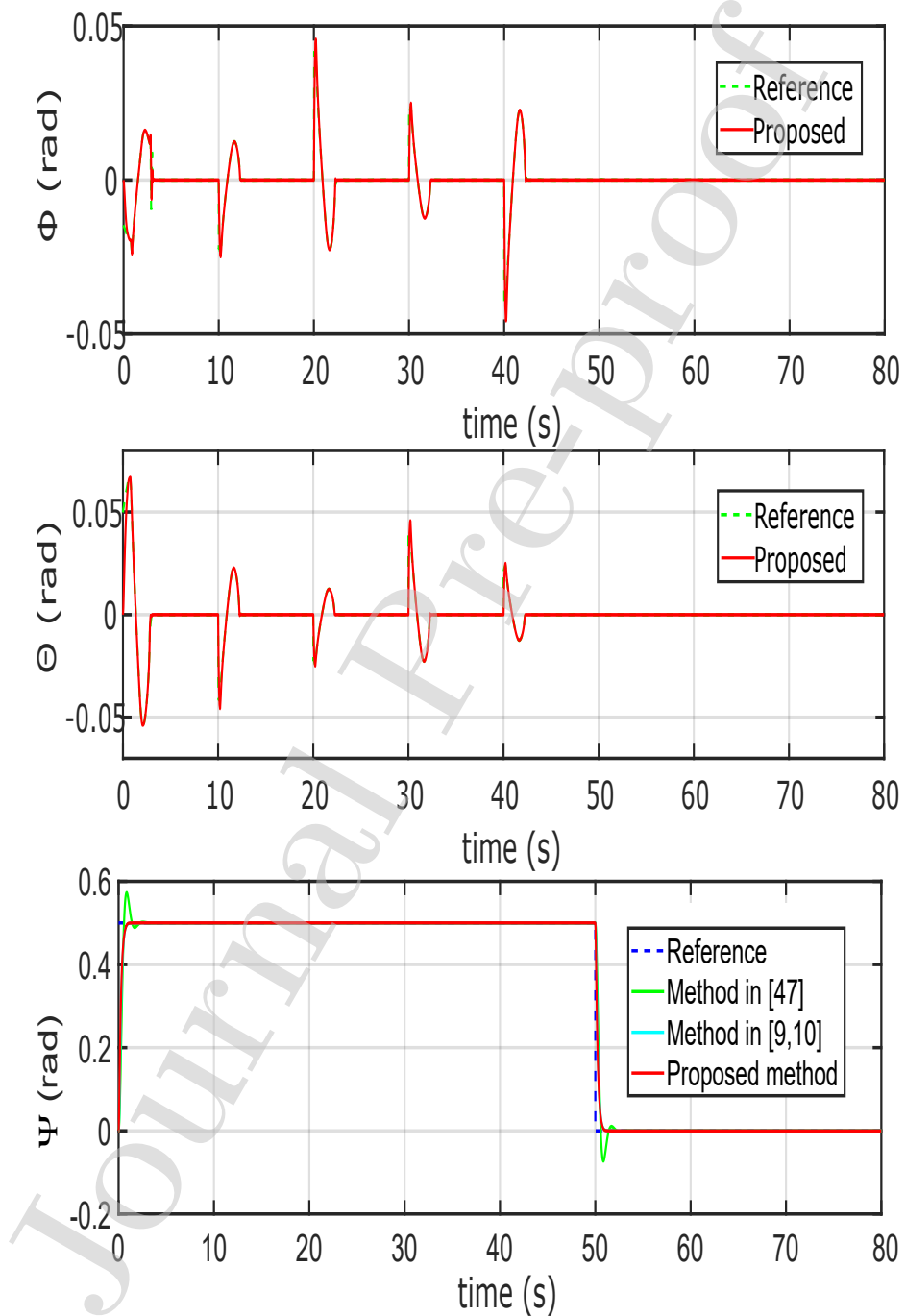
$$d_Z = \begin{cases} 0 & m/s^2 t \in [0, 25) \\ 1 & m/s^2 t \in [25, 40] \end{cases} \quad d_\Phi = \begin{cases} 0 & rad/s^2 t \in [0, 10) \\ 1 & rad/s^2 t \in [10, 40] \end{cases} \quad (71)$$

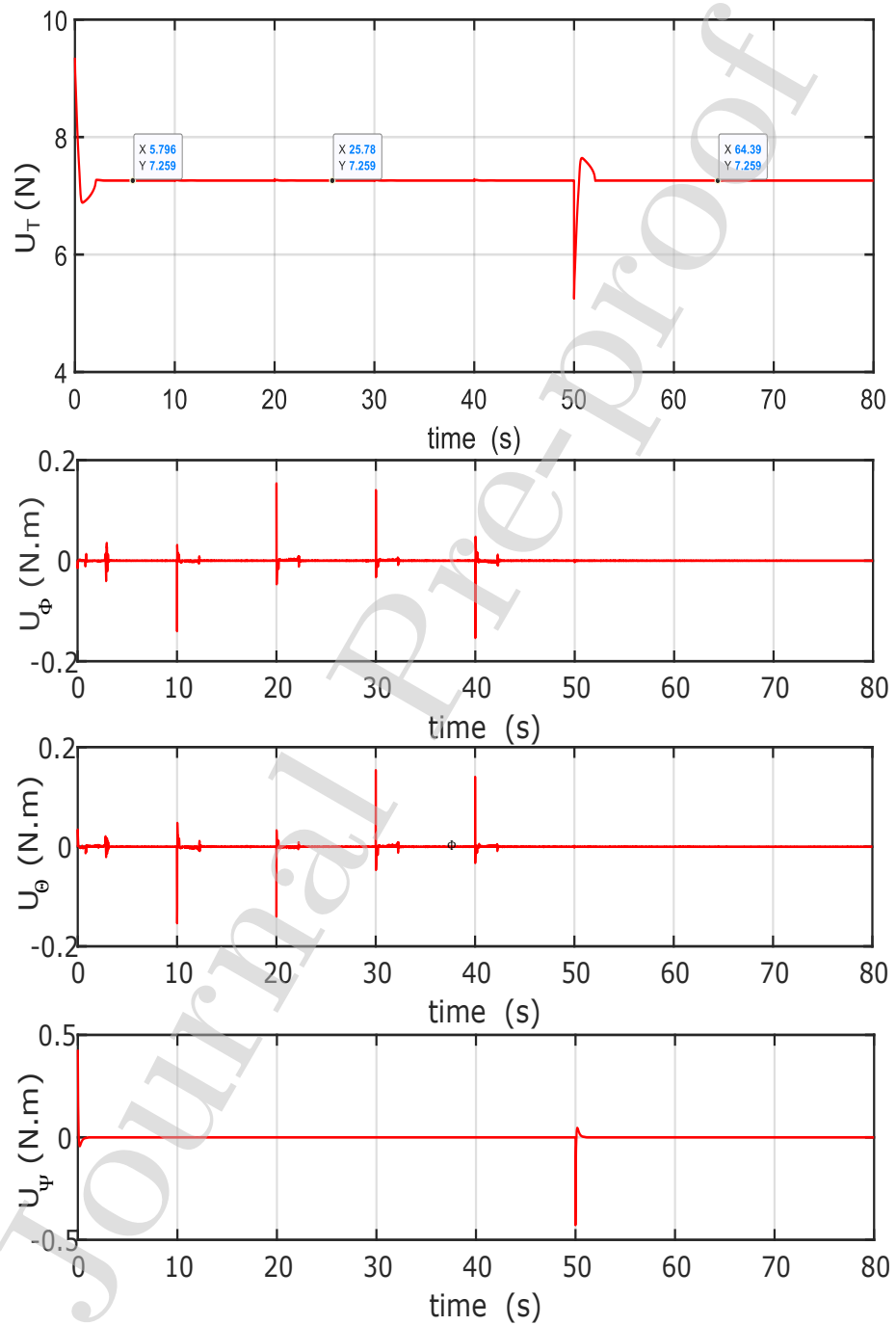
and

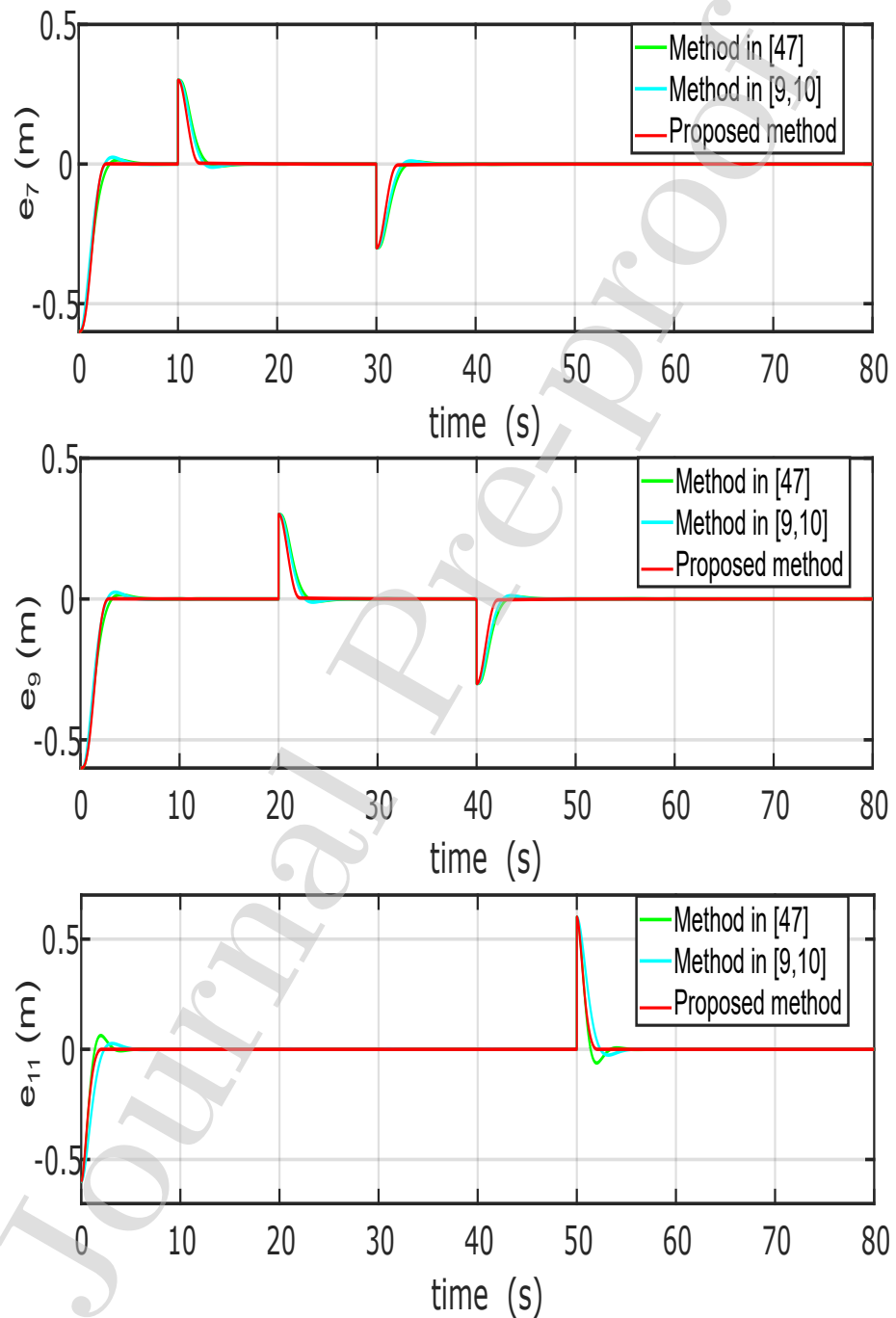
$$d_\Theta = \begin{cases} 0 & rad/s^2 t \in [0, 20) \\ 1 & rad/s^2 t \in [20, 40] \end{cases} \quad d_\Psi = \begin{cases} 0 & rad/s^2 t \in [0, 30) \\ 1 & rad/s^2 t \in [30, 40] \end{cases} \quad (72)$$

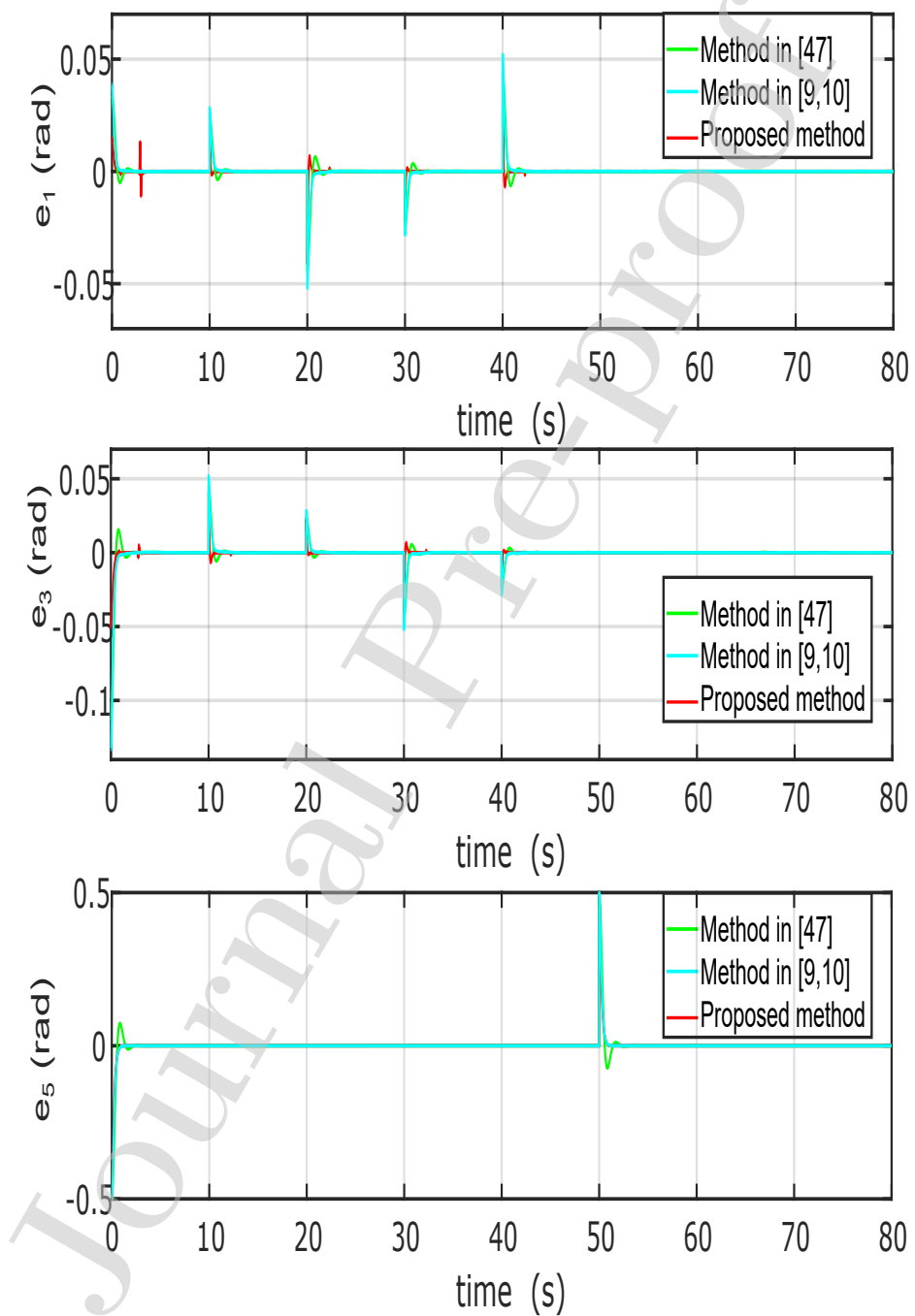
The position tracking results are illustrated in Figure 10. We see that the proposed control strategy successfully follows the position in the presence of disturbances. However, the BSMC and LF methods cannot provide good accuracy of the tracking of the desired position under sustained disturbances. The 3D trajectory tracking results are displayed in Figure 11. The perturbation is introduced at  $t = 10 \text{ s}$  for the position  $X$ , it can be observed that the ANFTSMC technique returns to the desired trajectory with no disturbances, the same for the position  $Y$  at  $t = 15 \text{ s}$ . This means that the RANFTSMC is

Figure 3: Quadrotor position ( $X, Y, Z$ ).

Figure 4: Quadrotor attitude ( $\Phi, \Theta, \Psi$ ).

Figure 5: Quadrotor inputs ( $U_T, U_\Phi, U_\Theta, U_\Psi$ ).

Figure 6: Tracking errors ( $e_7, e_9, e_{11}$ ) of the absolute position.

Figure 7: Tracking errors ( $e_1, e_3, e_5$ ) of the attitude angles.

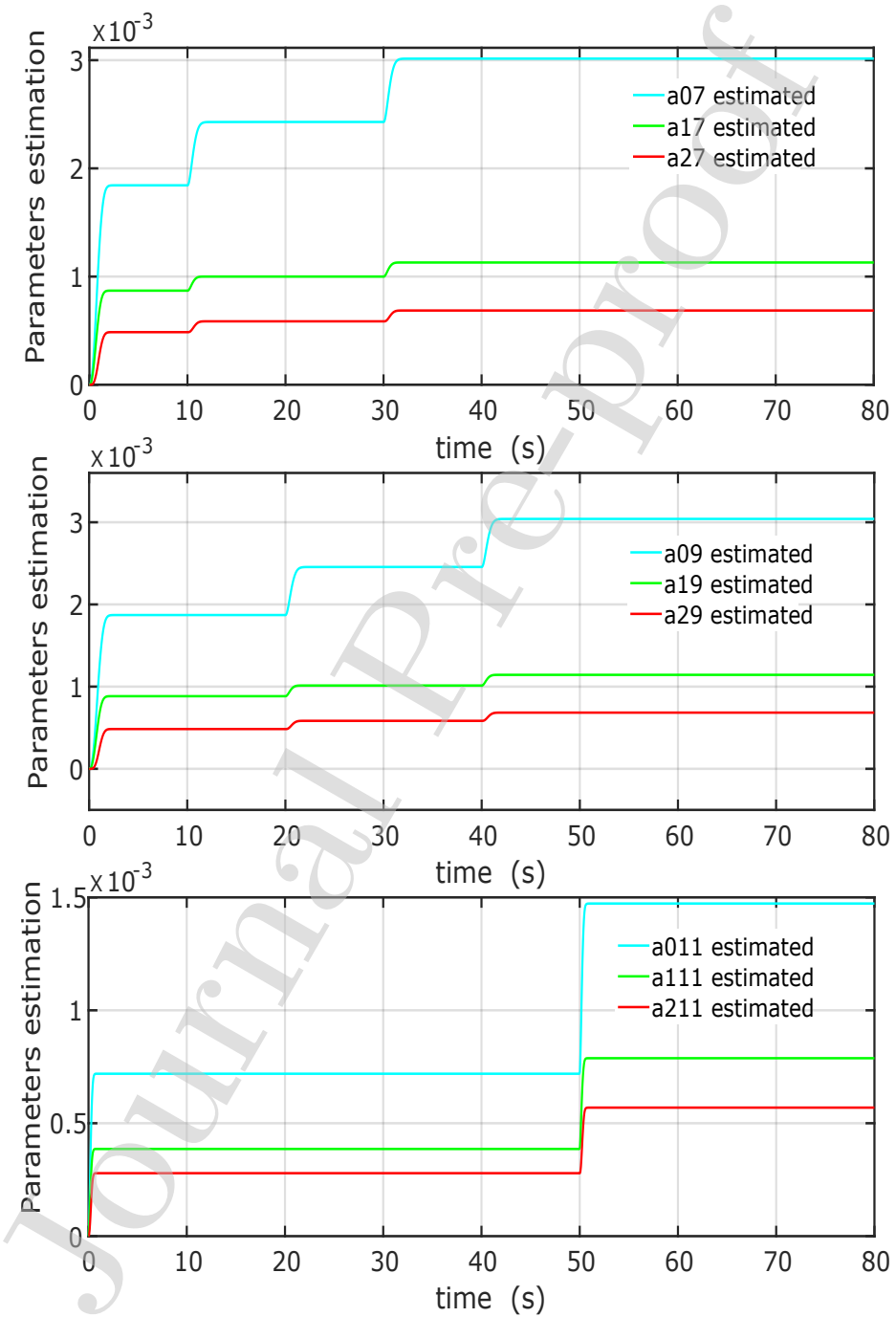


Figure 8: Position parameter estimation.

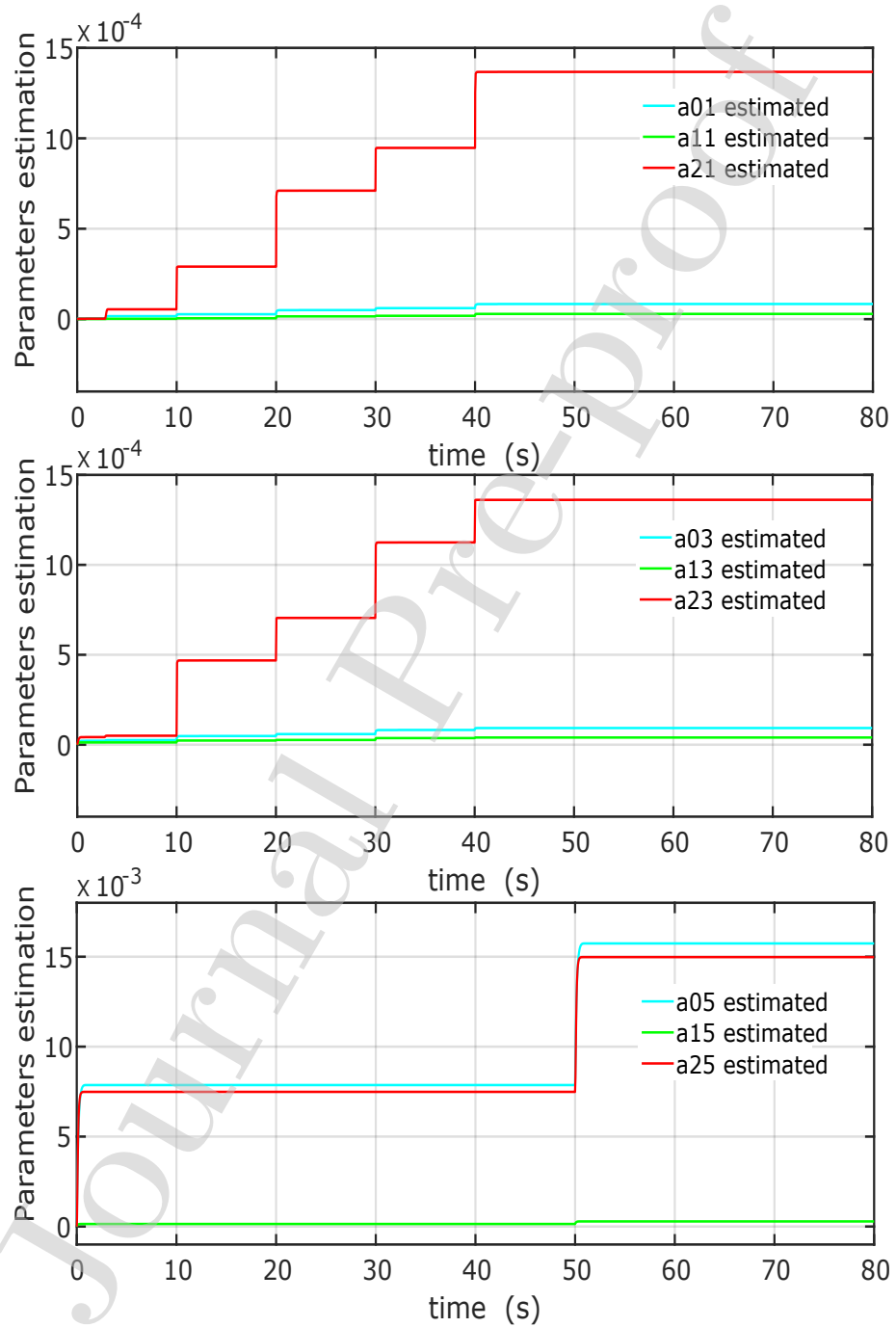


Figure 9: Position parameter estimation.

able to reject the disturbances. However, the FL and BSMC achieve the desired values of the quadrotor position and 3D flight trajectory just under undisturbed conditions (see Figures 10 and 11).

#### 4.3. Simulation 3

This part is dedicated for testing the stability of quadrotor while encountering time-varying disturbances. The perturbations are added to the quadrotor model equations. These disturbances are accelerations caused by gusts of wind when the quadrotor is flying outdoors [37]. Therefore, the expression of disturbances are as follows:

$$\begin{aligned}
 d_X = & - (0.8 \sin(0.1013t - 3.0403) + 0.4 \sin(0.4488t - 13.464) \\
 & + 0.08 \sin(1.5708t - 15\pi) + 0.056 \sin(0.2856t - 8.568)) \text{ m/s}^2 \quad t \in [10, 30] \\
 d_Y = & 0.5 \sin(0.4t) + 0.5 \cos(0.7t) \text{ m/s}^2 \quad t \in [10, 50] \\
 d_Z = & 0.5 \cos(0.7t) \text{ m/s}^2 \quad t \in [0, 80] \\
 d_\Phi = & 0.5 \cos(0.4t) \text{ rad/s}^2 \quad t \in [0, 80] \\
 d_\Theta = & 0.5 \sin(0.5t) \text{ rad/s}^2 \quad t \in [0, 80] \\
 d_\Psi = & 0.5 \sin(0.7t) \text{ rad/s}^2 \quad t \in [0, 80]
 \end{aligned} \tag{73}$$

The desired trajectory is given in Eqs. (74) and (75):

$$X_d = \begin{cases} \frac{1}{2} \cos(\frac{t}{2}) m & t \in [0, 4\pi) \\ 0.5 m & t \in [4\pi, 20) \\ 0.25t - 4.5 m & t \in [20, 30) \\ 3 m & t \in [30, 80] \end{cases} \quad Y_d = \begin{cases} \frac{1}{2} \sin(\frac{t}{2}) m & t \in [0, 4\pi) \\ 0.25t - 3.14 m & t \in [4\pi, 20) \\ 5 - \pi m & t \in [20, 30) \\ -0.2358t + 8.94 m & t \in [30, 40) \\ -0.5 m & t \in [40, 80] \end{cases} \tag{74}$$

$$Z_d = \begin{cases} 0.125t + 1 m & t \in [0, 4\pi) \\ 0.5\pi + 1 m & t \in [4\pi, 40) \\ \exp(-0.2t + 8.944) m & t \in [40, 80] \end{cases} \quad \Psi_d = 0 \text{ rad} \tag{75}$$

The initial conditions of the vehicle are: [0, 0, 0.5]rad and [0.5, 0.5, 0.5]m. The simulation is done under abrupt reference changes and time-varying disturbances. The proposed control strategy performances are shown in Figures 12

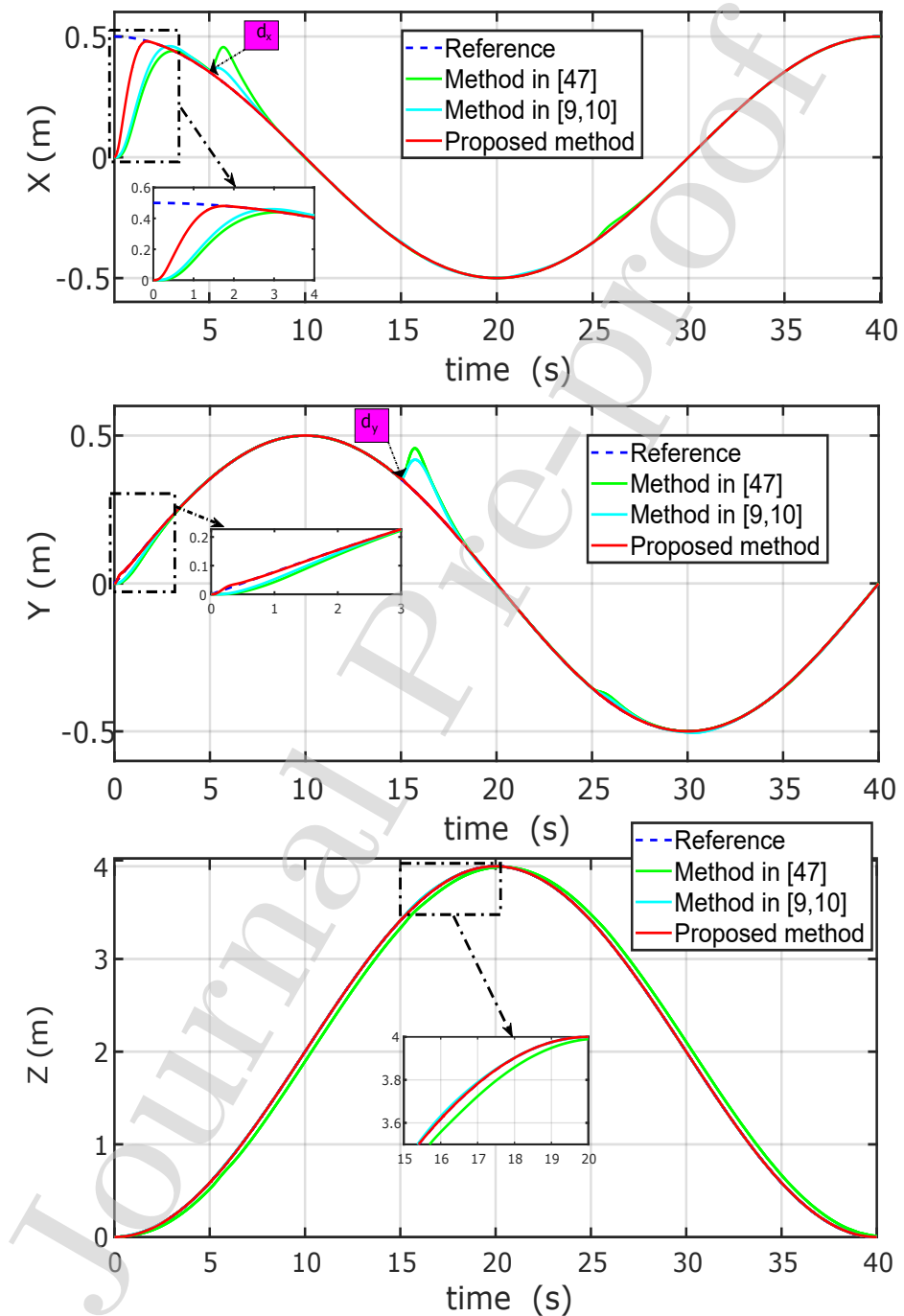


Figure 10: Quadrotor position ( $X, Y, Z$ ) under constant external disturbances.

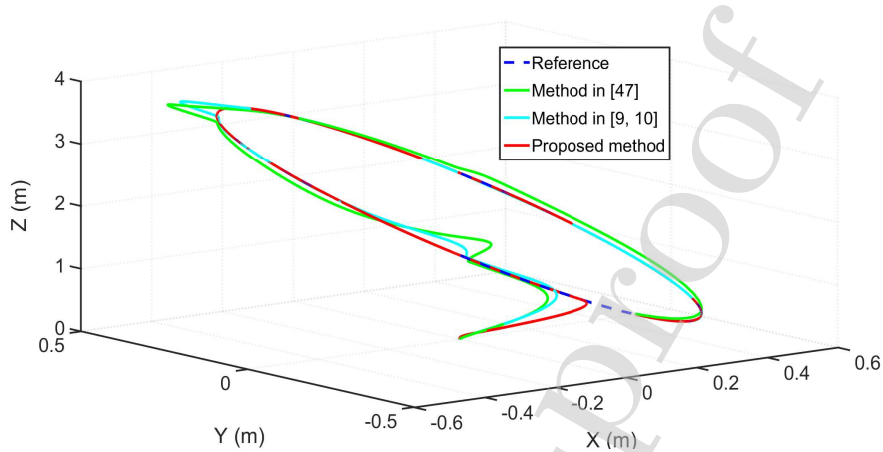


Figure 11: Flight trajectory tracking under constant external disturbances.

and 13. A comparison with the FL technique and BSMC proposed in Refs. [10, 9] are also given. The simulation results indicate that the robustness of the RANFTSMC approach against the complex disturbances is better than the other methods. Figure 12 depicts the position control performance. We see that the position controllers can accuracy track the desired values even if the references changes rapidly. Figure 13 shows the 3D desired flight trajectory. We observe from the aforementioned results that the ANFTSMC has well tracked the desired trajectory compared with other methods.

#### 4.4. Simulation 4

To further evaluate the performance of the RANFTSMC approach, the measurement noises effect are added to all state variables. This effect as displayed in Figure 14. The initial conditions of  $(\Phi, \Theta, \Psi, X, Y, Z)$  are:  $[0, 0, 0.5]$ rad and  $[0.5, 0.5, 0.5]$ m.

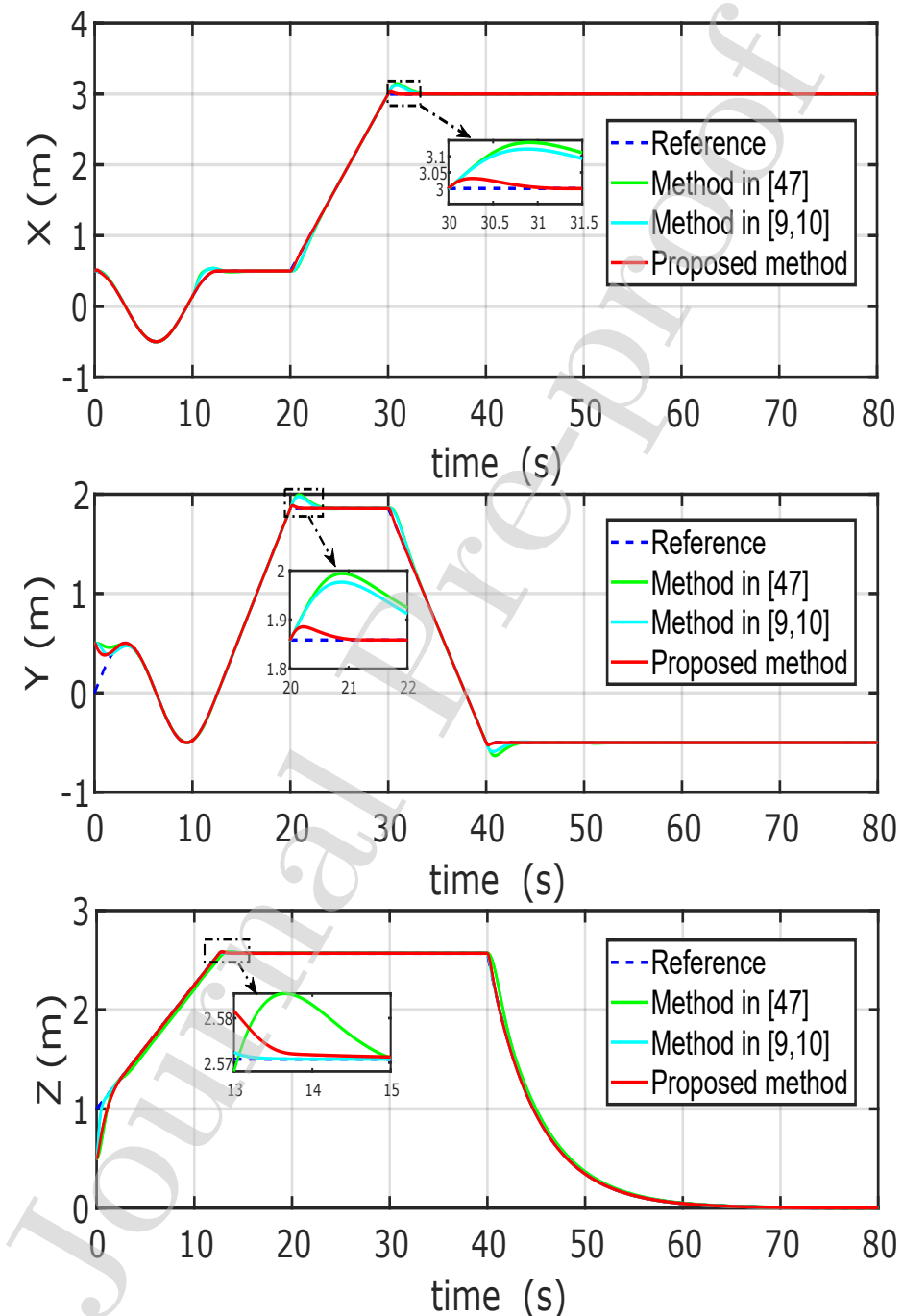


Figure 12: Quadrotor position ( $X, Y, Z$ ) under time-varying external disturbances.

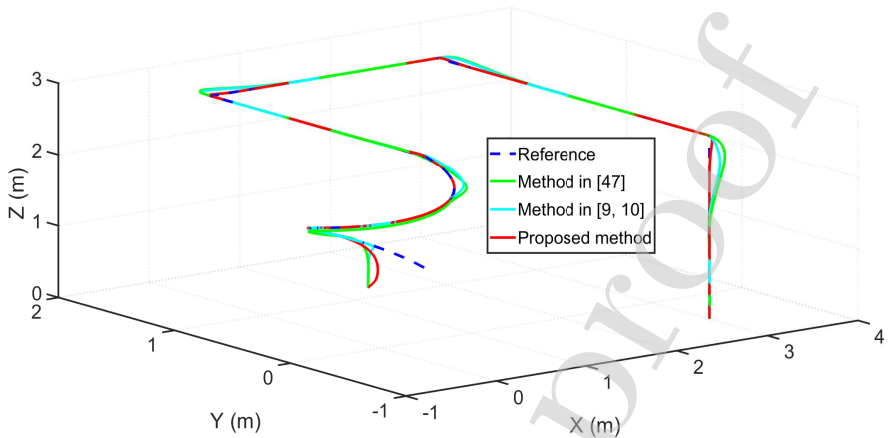


Figure 13: Flight trajectory tracking under time-varying external disturbances.

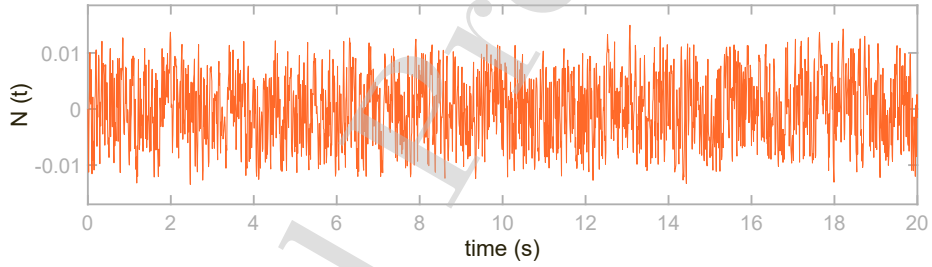


Figure 14: The measurement noise.

The simulation results of the RANFTSMC are indicated in [Figure 15](#) compared with the FL and BSMC methods. [Figure 15](#) shows the position trajectory. The performance results obtained by the proposed control present the worst profile compared to the other techniques (see [Figure 15](#)).

#### 4.5. Simulation 5

In this scenario, the moments of inertia, the aerodynamic coefficients, and the total mass are underrated  $\pm 50\%$  of the nominal values. Moreover, the simulation is done under time-varying disturbances. In addition, the RANFTSMC is compared with integral backstepping sliding mode controller (IBSMC) presented by the authors in Ref. [39]. The expression of the disturbances are given

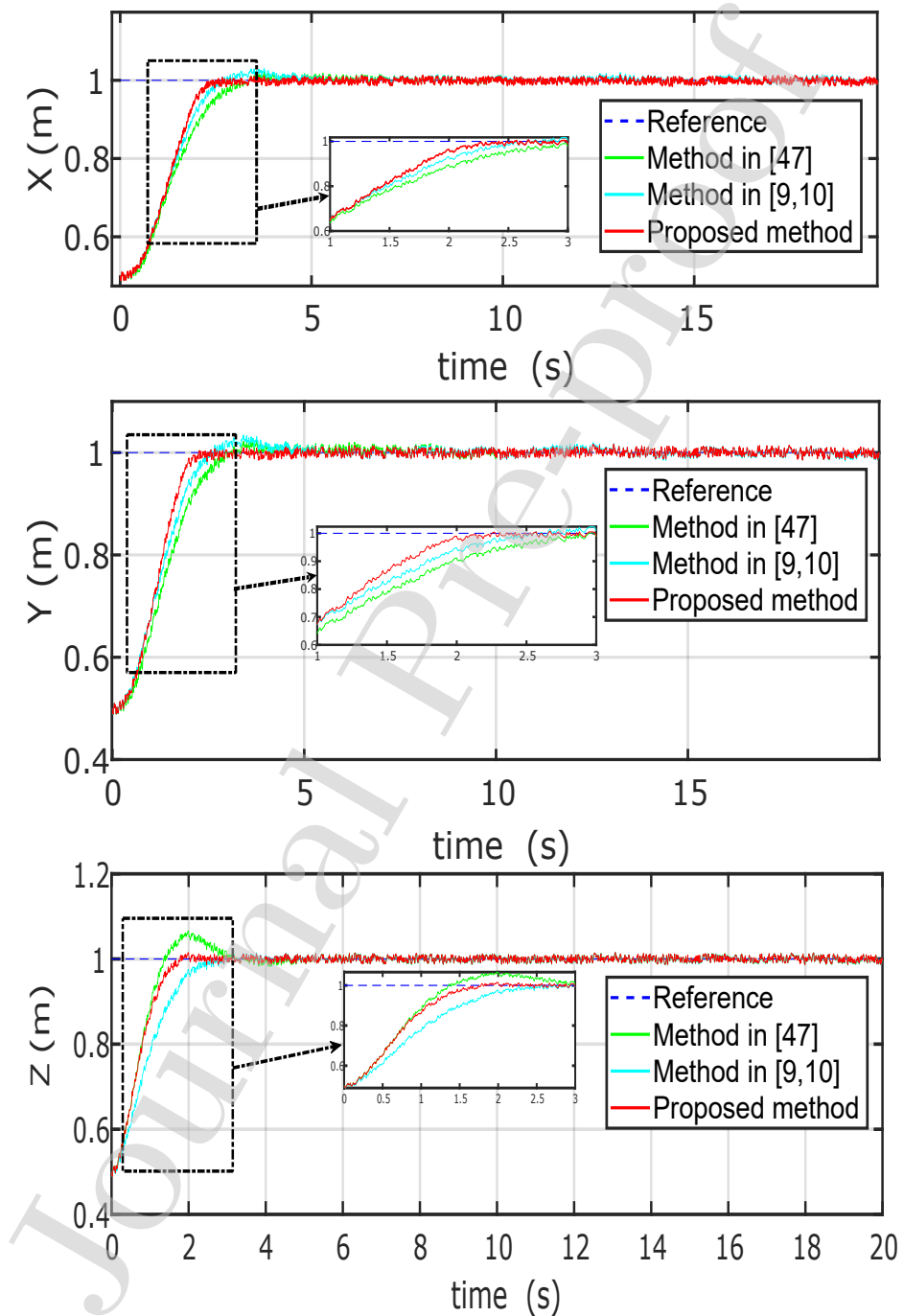


Figure 15: Quadrotor position ( $X, Y, Z$ ) in the case of measurement noise.

by:

$$\begin{aligned}
 d_X &= - (0.8 \sin(0.1013t - 3.0403) + 0.4 \sin(0.4488t - 13.464) \\
 &\quad + 0.08 \sin(1.5708t - 15\pi) + 0.056 \sin(0.2856t - 8.568)) \text{ m/s}^2 \quad t \in [10, 30] \\
 d_Y &= 0.5 \sin(0.4t) + 0.5 \cos(0.7t) \text{ m/s}^2 \quad t \in [10, 50] \\
 d_Z &= 0.5 \cos(0.7t) + 0.7 \sin(0.3t) \text{ m/s}^2 \quad t \in [0, 120] \\
 d_\Phi &= 0.5 \cos(0.4t) + 1 \text{ rad/s}^2 \quad t \in [0, 120] \\
 d_\Theta &= 0.5 \sin(0.5t) + 1 \text{ rad/s}^2 \quad t \in [0, 120] \\
 d_\Psi &= 0.5 \sin(0.7t) + 1 \text{ rad/s}^2 \quad t \in [0, 120]
 \end{aligned} \tag{76}$$

The desired space trajectory is given as:

$$X_d = \begin{cases} 0 & t \in [0, 55) \\ 0.3 \cos(\frac{\pi t}{6}) \text{ m} & t \in [55, 120] \end{cases} \quad Y_d = \begin{cases} 0 & t \in [0, 55) \\ 0.3 \sin(\frac{\pi t}{6}) \text{ m} & t \in [55, 120] \end{cases} \tag{77}$$

$$Z_d = \begin{cases} 0.5 \text{ m} & t \in [0, 42) \\ 0.7 \text{ m} & t \in [42, 87) \\ 0.8 \text{ m} & t \in [87, 120] \end{cases} \quad \Psi_d = 0 \text{ rad} \tag{78}$$

The initial conditions of the attitude and position are  $[0, 0, 0.5]$ rad and  $[0.5, 0.5, 0.5]$ m. The tracking performances under the time-varying disturbances and parametric uncertainties are plotted in Figures 16 and 17, as can be seen the results obtained have an excellent tracking of the proposed trajectory. The RANFTSMC technique allows the attitude loop stabilization under perturbations and parametric uncertainties (see Figures 16 and 17). The quadrotor can maintain the desired  $X$  and  $Y$  positions with a good accuracy compared with IBSMC approach presented in Ref. [39] during the first period  $(0, 55)$  of the flight. Besides, the altitude of the IBSMC method has high oscillations and overshoots during the disturbed period of the desired altitude. Therefore, It is worth-while to note that the proposed RANFTSMC is able to reject the perturbations. Moreover, it is clear from Figure 16 that the proposed approach gives excellent results for the tracking trajectory with  $50 \pm \%$  uncertainty of the quadrotor parameters and the disturbances. The result of the proposed inner controller, which allows to the quadrotor to follow the reference angles, is

presented in [Figure 17](#). Here, we can see that the quadrotor system is highly-coupled. Each subsystem is affected by different disturbance (see Eq. [\(76\)](#)). Therefore, any change of the quadrotor parameters can cause a change of the roll and the pitch angle references. Clearly, we can observe that the proposed RANFTSMC can accurately track the desired yaw, roll, and pitch angles.

A quantitative comparison between the proposed RANFTSMC, FL and BSMC methods are considered based on the integral square error (ISE) performance indexes defined in Ref. [\[37\]](#) as follows:

$$ISE = \int_{t_i}^{t_f} e^2 dt \quad (79)$$

where  $t_f$  and  $t_i$  denote the final and initial instants, respectively and  $e$  represents the tracking error.

The results are presented in [Table 4](#). The RANFTSMC method is significantly superior to the FL and BSMC control approaches, which can be observed in [Table 4](#), the proposed RANFTSMC supplied a more accurate tracking even under the sensor noises and time-varying disturbances.

**Remark 3.** *The ISE values shown in [Table 4](#) are obtained from [subsection 4.2](#).*

Similarly, [Table 5](#) shows a comparative based on ISE performance indexes between the proposed RANFTSMC technique and IBSMC method. We can observe, from [Table 5](#) that the proposed approach remains the best one and has an excellent ISE compared to IBSMC. Finally, the proposed controller has an excellent tracking of the flight trajectory and strong robustness in all proposed scenarios. The simulation results have proved that the RANFTSMC has a better tracking performance than FL, BSM, and IBSM control methods. Due to the adaptive mechanism ability provided by RANFTSMC and strong robustness of proposed RANTSMC, parametric uncertainties, external disturbances, and measurement noise are well compensated with the RANFTSM controller.

Table 4: ISE performance indexes.

State	FL	BSMC	Proposed RANFTSMC
$x$	0.2995	0.2525	0.1295
$y$	0.0255	0.0175	1.322e-05
$z$	0.2239	0.0002	5.782e-07
$\phi$	0.0064	0.0034	0.0019
$\theta$	0.0079	0.0030	0.0015
$\psi$	0.0572	0.0438	0.1485

Table 5: ISE performance indexes.

State	Proposed RANFTSMC	IBSMC
$x$	0.1551	0.1851
$y$	0.1253	0.1665
$z$	0.0193	0.00245
$\phi$	0.0093	4.638
$\theta$	0.0090	4.699
$\psi$	0.1495	8.969

**Remark 4.** This note goes at describing the procedure for experimental validation of the proposed control approach [49, 50]. A list of the pieces of equipment has been compiled to build a drone test bench experimental that can test and verify the proposed scenarios. The hardware configuration of the unmanned aircraft vehicle experimental platform is shown in [Figure 18](#). It is a quadrotor of version X450 with one ground control station (GCS). The flight control system is based on DSP TMS320F28377S. The Inertial Measurement Unit (IMU) includes 3-axis gyroscope, 3-axis magnetometer, and 3-axis accelerometer. The global positioning system (GPS) module measures the velocity and position in the horizontal plane. A magnetometric sensor and a barometric sensor measure the altitude. Moreover, two Zigbee wireless modules ensure the communication

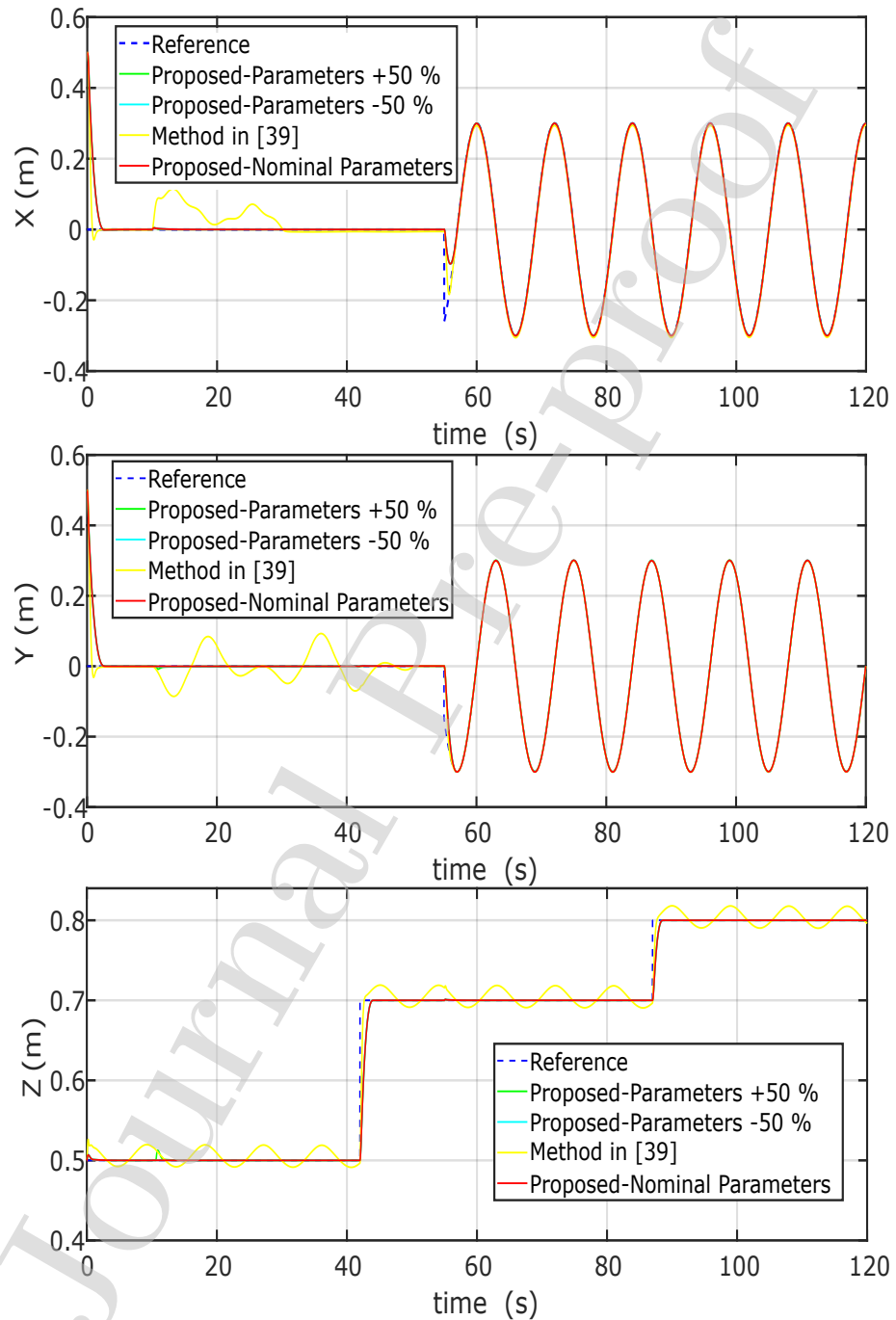


Figure 16: Quadrotor position ( $X, Y, Z$ ) under external disturbances and parameters uncertainties.

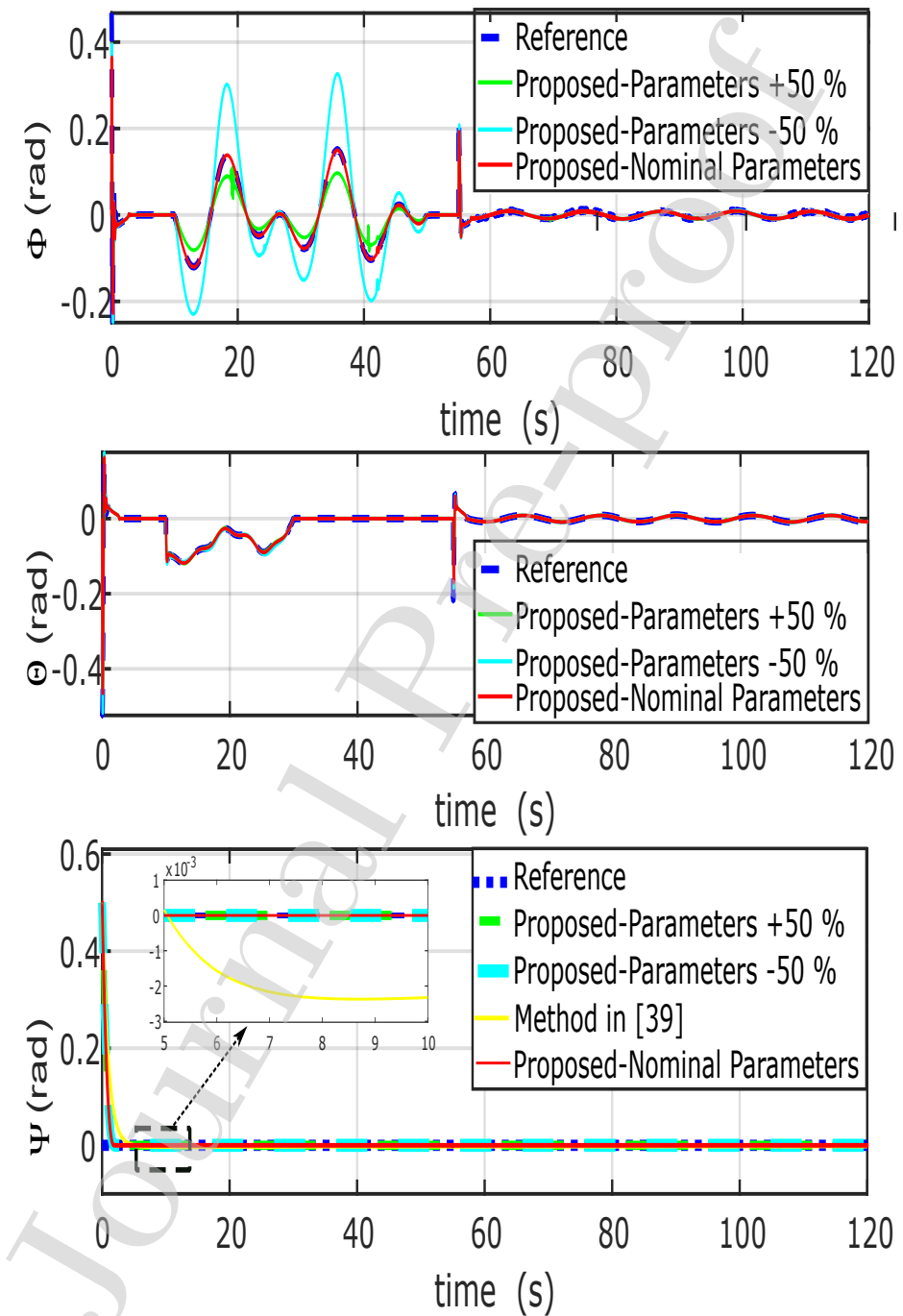


Figure 17: Quadrotor attitude ( $\Phi, \Theta, \Psi$ ) under external disturbances and parameters uncertainties

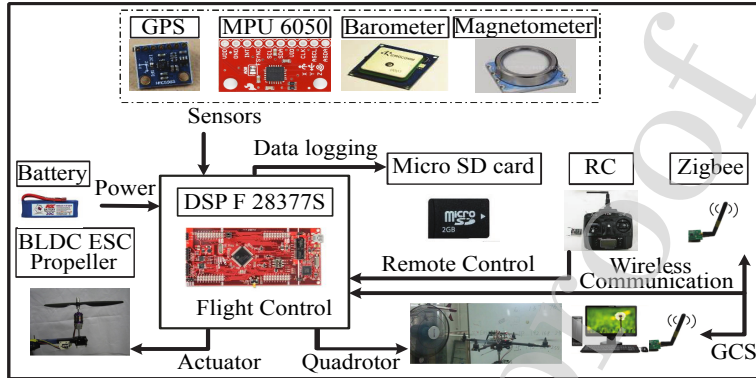


Figure 18: The quadrotor's hardware structure.

*between the quadrotor and the ground station. A fan generates the wind then applied as an external disturbance to the quadrotor. A micro SD card saves the flight parameters onboard.*

## 5. Conclusion

In this work, based on the laws of physics (Lagrange-Euler and Newton-Euler), a mathematical model of the quadrotor rotational and translational is obtained. A novel RANFTSMC technique is suggested to address the trajectory tracking control problem of an uncertainty quadrotor under disturbances. Furthermore, the fast convergence of all state variables was achieved and the influence of the chattering effect in SMC was eliminated, while the online estimation of the parameters was presented and the singularity problem of TSMC was avoided. The efficiency of the proposed RANFTSMC approach was demonstrated in multiple test scenarios (Constant external disturbances, parametric uncertainties, measurement noise, and time-varying external disturbances). Simulation results illustrate that the RANFTSMC approach proposed in this work has a good tracking of the desired trajectory, fast finite-time convergences of sliding surfaces with higher precision, a null steady-state of the tracking errors, and high level of robustness against external perturbations compared to

backstepping SM, integral backstepping SM, and feedback linearization control methods.

For further work, the RANFTSMC will be validated by experiment. Design a fractional-order RANFTSM control technique to improve the performances of RANFTSMC method. Also, the fault-tolerant control problem of the quadrotor actuators and sensors will be addressed.

## References

- [1] M. Hassanalian, A. Abdelkefi, Classifications, applications, and design challenges of drones: A review, *Progress in Aerospace Sciences*[J], 91 (2017), pp. 99131.
- [2] C. Kanellakis, G. Nikolakopoulos, Survey on Computer Vision for UAVs: Current Developments and Trends, *Journal of Intelligent & Robotic Systems*[J], 87 (2017), pp. 141168.
- [3] C. Wang, B. Song, P. Huang, Trajectory Tracking Control for Quadrotor Robot Subject to Payload Variation and Wind Gust Disturbance, *Journal of Intelligent & Robotic Systems*[J], (2016) doi: 10.1007/s10846-016-0333-4.
- [4] H. Liu, J. Xi, Y. Zhong, Robust Attitude Stabilization for Nonlinear Quadrotor Systems with Uncertainties and Delays, *IEEE Transactions on Industrial Electronics*[J], 64 (2017), pp. 55855594.
- [5] O. Mofid, S. Mobayen, Adaptive sliding mode control for finite-time stability of quadrotor UAVs with parametric uncertainties, *ISA Transactions*[J], 72 (2018), pp. 114.
- [6] X. Shao, J. Liu, H. Wang, Robust back-stepping output feedback trajectory tracking for quadrotors via extended state observer and sigmoid tracking differentiator, *Mechanical Systems and Signal Processing*[J], 104 (2018), pp. 631647.

- [7] R. Ayad, et al. Full Control of Quadrotor Aerial Robot Using Fractional-Order FOPID, Iranian Journal of Science and Technology[J], Transactions of Electrical Engineering, 43 (2019)(Suppl 1): 349.
- [8] Y. Bouzid, H. Siguierdidjane, Y. Bestaoui, Energy based 3D trajectory tracking control of quadrotors with model-free based on-line disturbance compensation, Chinese Journal of Aeronautics[J], 31 (2018), pp. 15681578.
- [9] M. A. M. Basri, Design and application of an adaptive backstepping sliding mode controller for a six-DOF quadrotor aerial robot, Robotica[J], 36 (2018), pp. 17011727.
- [10] F. Chen, et al., Robust Backstepping Sliding Mode Control and Observer-Based Fault Estimation for a Quadrotor UAV, IEEE Transactions on Industrial Electronics[J], 63 (2016), pp. 5044-5056.
- [11] A. Castillo, et al., Disturbance observer-based quadrotor attitude tracking control for aggressive maneuvers, Control Engineering Practice[J], 82 (2019), pp. 1423.
- [12] H. Rios, et al. Continuous Sliding-Mode Control Strategies for Quadrotor Robust Tracking: Real-Time Application, IEEE Transactions on Industrial Electronics[J], 66 (2019), pp. 12641272.
- [13] D. Ma, et al., Flatness-based adaptive sliding mode tracking control for a quadrotor with disturbances, Journal of the Franklin Institute[J], 355 (2018), pp. 63006322.
- [14] F. Muoz, et al., Second order sliding mode controllers for altitude control of a quadrotor UAS: Real-time implementation in outdoor environments, Neurocomputing[J], 233 (2016), pp. 6171.
- [15] S. Li, Y. Wang, Y. Tan, Adaptive and robust control of quadrotor aircrafts with input saturation, Nonlinear Dynamics[J], 89 (2017), pp. 255265.

- [16] A. Dzul, et al., Nonlinear PID-Type Controller for Quadrotor Trajectory Tracking, IEEE/ASME TRANSACTIONS ON MECHATRONICS[J], 4435 (2018), pp. 111.
- [17] C. Hua, J. Chen, X. Guan, Fractional-order sliding mode control of uncertain QUAVs with time-varying state constraints, Nonlinear Dynamics[J], 95 (2018), pp. 13471360.
- [18] J. J. Xiong, G. B. Zhang, Global fast dynamic terminal sliding mode control for a quadrotor UAV, ISA Transactions[J], 66, (2017) pp. 233240.
- [19] H. Mo, G. Farid, Nonlinear and Adaptive Intelligent Control Techniques for Quadrotor UAV - A Survey, Asian Journal of Control[J], 21 (2018), pp. 120.
- [20] U. Ansari, A. H. Bajodah, M. T. Hamayun, Quadrotor Control Via Robust Generalized Dynamic Inversion and Adaptive Non-Singular Terminal Sliding Mode, Asian Journal of Control[J], 21 (2018), pp. 113.
- [21] G. V. Raffo, M.G. Ortega, FR. Rubio, An integral predictive/nonlinear  $H\infty$  control structure for a quadrotor helicopter. Automatica[J], 46 (2010), pp. 2939.
- [22] G. V. Raffo, M.G. Ortega, FR. Rubio, Robust nonlinear control for path tracking of a quadrotor helicopter, Asian Journal of Control[J], 17 (2015), pp. 14256.
- [23] E. H. Zheng, J. J. Xiong, J. L. Luo, Second order sliding mode control for a quadrotor UAV, ISA Transactions[J]. , 53 (2014), pp. 13501356.
- [24] S. Jalili, B. Rezaie, Z. Rahmani, A novel hybrid model predictive control design with application to a quadrotor helicopter, Optimal Control Applications and Methods, (2018), pp. 122.
- [25] B. Tian, et al., Multivariable finite-time output feedback trajectory tracking control of quadrotor helicopters, International Journal of Robust and Nonlinear Control[J], 28 (2017), pp. 281-295.

- [26] Y. Zhang, et al., A novel control scheme for quadrotor UAV based upon active disturbance rejection control, Aerospace Science and Technology[J], 79 (2018), pp. 601609.
- [27] M. A. Modirrousta, A. Khodabandeh, Novel Nonlinear Hybrid Controller Design for an Uncertain Quadrotor with Disturbances, Aerospace Science and Technology[J], 45 (2015), pp. 294-308.
- [28] D. Invernizzi, M. Lovera, Trajectory tracking control of thrust-vectoring UAVs, Automatica, 95 (2018), pp. 180186.
- [29] I. A. A. Prado, et al., Experimental evaluation of HJB optimal controllers for the attitude dynamics of a multirotor aerial vehicle, ISA Transactions[J], 77, (2018) pp. 188200.
- [30] J. Chang, et al., Analysis and design of second-order sliding-mode algorithms for quadrotor roll and pitch estimation, ISA Transactions[J], 71 (2017), pp. 495-512.
- [31] M. E. Guerrero-snchez, et al., Swing-attenuation for a quadrotor transporting a cable-suspended payload, ISA Transactions[J], 68 (2017) pp. 433-449.
- [32] M. Shirzadeh et al., An indirect adaptive neural control of a visual-based quadrotor robot for pursuing a moving target, ISA Transactions[J], 59 (2015), pp. 290-302.
- [33] N. Wang, et al., Hybrid finite-time trajectory tracking control of a quadrotor, ISA Transactions[J], 90 (2019), pp. 278-286.
- [34] E. Slawiski, D. Santiago, V. Mut, Control for delayed bilateral teleoperation of a quadrotor, ISA Transactions[J], 71 (2017), pp. 415425.
- [35] J. Xiong, E. Zheng, Position and attitude tracking control for a quadrotor UAV, ISA Transactions[J], 53 (2014), pp. 725-73.
- [36] Z. Li, X. Ma , Y. Li, Robust tracking control strategy for a quadrotor using RPD-SMC and RISE. Neurocomputing[J], 331 (2018) pp. 312322.

- [37] Y. Bouzid, H. Siguerdidjane, Y. Bestaoui, Nonlinear internal model control applied to VTOL multi-rotors UAV. Mechatronics[J] 47 (2017), pp. 4966.
- [38] S. Bouabdallah, A. Noth, R. Siegwan, PID vs LQ Control Techniques Applied to an Indoor Micro Quadrotor, IEEE International Conference on Intelligent Robots and Systems[C] ( 2004) pp. 24512456.
- [39] Z. Jia, et al., Integral backstepping sliding mode control for quadrotor helicopter under external uncertain disturbances, Aerospace Science and Technology[J], 68 (2017), pp. 299307.
- [40] M. Labbadi, et al., A Comparative Analysis of Control Strategies for Stabilizing a Quadrotor, Smart Innovation, Systems and Technologies[C], 111 (2019), pp. 625-630.
- [41] M. Labbadi, M. Cherkouci, Robust adaptive backstepping fast terminal sliding mode controller for uncertain quadrotor UAV, Aerospace Science and Technology[J], 93 (2019), pp. 105306.
- [42] M. Boukattaya, et al., Adaptive nonsingular fast terminal sliding-mode control for the tracking problem of uncertain dynamical systems, ISA Transactions[J], 77 (2018), pp. 1-19.
- [43] P. Lin, J. Ma, Z. Zheng, Robust adaptive sliding mode control for uncertain nonlinear MIMO system with guaranteed steady state tracking error bounds, Journal of the Franklin Institute[J], 353 (2016), pp. 303-321.
- [44] M. Zhihong, X. Yu, Adaptive terminal sliding mode tracking control for rigid robotic manipulators with uncertain dynamics, JSME International Journal Series C Mechanical Systems, Machine Elements and Manufacturing[J], 40 (1997), pp. 493-502.
- [45] L. Yang, J. Yang, Nonsingular fast terminal sliding-mode control for nonlinear dynamical systems. International Journal of Robust and Nonlinear Control[J], 21 (2016), 1865-1879.

- [46] S. B. Fazeli Asl, S. S. Moosapour, Adaptive backstepping fast terminal sliding mode controller design for ducted fan engine of thrust-vector aircraft, Aerospace Science and Technology[J], 71 (2017), pp. 521529.
- [47] H. Voos, Nonlinear control of a quadrotor micro-uav using feedback-linearization, IEEE International Conference on Mechatronics[C], 2009.
- [48] F. P. Freire, N. A. Martins, F. Splendor, A Simple Optimization Method for Tuning the Gains of PID Controllers for the Autopilot of Cessna 182 Aircraft Using Model-in-the-Loop Platform, Journal of Control, Automation and Electrical Systems[J], 29(2018), pp. 441450.
- [49] Y. Yu, X. A Ding, Quadrotor Test Bench for Six Degree of Freedom Flight, Journal of Intelligent & Robotic Systems[J], 68 (2012), pp. 323338.
- [50] X. Dong, et al., Time-Varying Formation Tracking for Second-Order Multi-Agent Systems Subjected to Switching Topologies With Application to Quadrotor Formation Flying, IEEE Transactions on Industrial Electronics[J], 64 (2017), pp. 50145024.

\*Conflict of Interest

CONFLICT OF INTEREST

The authors declare that they have no conflict of interest.